Biochimica et Biophysica Acta 1852 (2015) 2145–2160

Contents lists available at ScienceDirect

Biochimica et Biophysica Acta

journal homepage: www.elsevier.com/locate/bbadis

Cdk5-mediated mitochondrial fission: A key player in dopaminergic toxicity in Huntington's disease

Marta Cherubini, Mar Puigdellívol, Jordi Alberch, Silvia Ginés *

Departament de Biologia Cel·lular, Immunologia i Neurociències, Facultat de Medicina, Universitat de Barcelona, Barcelona, Spain
Institut d'Investigacions Biomèdiques August Pi i Sunyer (IDIBAPS), Barcelona, Spain
Centro de Investigación Biomédica en Red sobre Enfermedades Neurodegenerativas (CIBERNED), Spain

ARTICLE INFO

Article history:
Received 11 March 2015
Received in revised form 18 June 2015
Accepted 29 June 2015
Available online 2 July 2015

Keywords:
Cdk5
Dopaminergic activation
Drp1
Huntingtin
Mitochondrial dynamics

ABSTRACT

The molecular mechanisms underlying striatal vulnerability in Huntington's disease (HD) are still unknown. However, growing evidence suggest that mitochondrial dysfunction could play a major role. In searching for a potential link between striatal neurodegeneration and mitochondrial defects we focused on cyclin-dependent kinase 5 (Cdk5). Here, we demonstrate that increased mitochondrial fission in mutant huntingtin striatal cells can be a consequence of Cdk5-mediated alterations in Drp1 subcellular distribution and activity since pharmacological or genetic inhibition of Cdk5 normalizes Drp1 function ameliorating mitochondrial fragmentation. Interestingly, mitochondrial defects in mutant huntingtin striatal cells can be worsened by D1 receptor activation a process also mediated by Cdk5 as down-regulation of Cdk5 activity abrogates the increase in mitochondrial fission, the translocation of Drp1 to the mitochondria and the raise of Drp1 activity induced by dopaminergic stimulation. In sum, we have demonstrated a new role for Cdk5 in HD pathology by mediating dopaminergic neurotoxicity through modulation of Drp1-induced mitochondrial fragmentation, which underscores the relevance for pharmacologic interference of Cdk5 signaling to prevent or ameliorate striatal neurodegeneration in HD.

1. Materials and methods

1.1. Cell cultures

Conditionally immortalized wild-type ST7/7Q and mutant ST111/111Q striatal neuronal progenitor cell lines expressing endogenous levels of normal and mutant huntingtin with 7 and 111 glutamines, respectively, have been described previously [1]. Striatal cells were grown at 33 °C in Dulbecco's modified Eagle's medium (DMEM, Sigma-Aldrich; St. Louis, MO, USA), supplemented with 10% fetal bovine serum, 1% penicillin–streptomycin, 2 mM L-glutamine, 1 mM sodium pyruvate and 400 μg/ml G418 (Geneticin; GIBCO-BRL, Life technologies; Gaithersburg, MD, USA).

1.2. Primary cultures of mouse striatal neurons

Dissociated striatal cultures prepared from E.18 Hdh7/7Q and Hdh7/111Q embryos were plated at a density of 40,000 neurons onto 24-well plates pre-coated with 0.1 mg/ml poly-D-lysine (Sigma Chemical Co., St. Louis, MO). Neurons were cultured in Neurobasal medium (Gibco-BRL, Renfrewshire, Scotland, UK), supplemented with B27 (Gibco-BRL) and GlutamaxTM (Gibco-BRL). Cultures were maintained at 37 °C in a humidified atmosphere containing 5% CO_2.

1.3. HD mouse models

HdhQ111 knock-in mice, with targeted insertion of 109 CAG repeats that extends the glutamine segment in murine huntingtin to 111 residues, were maintained on a C57BL/6 genetic background. Male and female Hdh7/111Q heterozygous mice were intercrossed to generate age-matched Hdh7/111Q heterozygous and Hdh7/7Q wild-type littermates. The animals were housed with access to food and water ad libitum in a colony room kept at 19–22 °C and 40–60% humidity, under a 12:12 h light/dark cycle. Only males were used to perform all the experiments. All procedures were performed in compliance with the National Institutes of Health Guide for the Care and Use of Laboratory Animals, and approved by the local animal care committee of the Universitat de Barcelona (99/01) and Generalitat de Catalunya (00/1094), in accordance with the Directive 2010/63/EU of the European Commission.

1.4. Drug treatment

To assess the effect of dopamine receptor activation on mitochondrial population, striatal cell lines were treated as previously described [2].

* Corresponding author at: Universitat de Barcelona, Casanova 143, E-08036 Barcelona, Spain.
E-mail address: silviagines@ub.edu (S. Ginés).

http://dx.doi.org/10.1016/j.bbadis.2015.06.025
0925-4439/

Briefly, wild-type ST7/7Q and mutant ST111/111Q striatal cells were serum depleted (2.5% FBS) for 24 h and then exposed to Locke's solution (154 mM NaCl, 5.6 mM KCl, 2.3 mM CaCl2, 3.6 mM NaHCO3, 5 mM HEPES, 5.6 mM glucose, and 10 μM glycine) for 30 min before the addition of SKF 38393, 30 or 60 μM (Sigma Aldrich) in fresh DMEM medium (2.5% FBS). To prevent SKF 38393 effect, cultures were treated with the D1 receptor antagonist SCH 23390 10 μM (Sigma Aldrich) 1 h before SKF 38393 treatments. Total extracts were obtained 60 min after SKF 38393 treatment for later analysis. To inhibit Cdk5 activity, cultures were treated with the Cdk5 inhibitor roscovitine, 20 μM (Sigma-Aldrich) 1 h before SKF 38393 treatments. Cells were then fixed for later analysis.

1.5. Cell transfection

Cells were transiently transfected using Lipofectamine 2000 (Invitrogen, Life Technologies) according to the manufacturer's instructions and incubated for 48 h before use. To suppress Cdk5 expression, cells were transfected with the appropriate antisense oligonucleotides (sc-35047; Santa Cruz Biotechnology, Santa Cruz, CA) or with a scramble control (sc-37007; Santa Cruz Biotechnology) and harvested for Western blot or fixed for immunocytochemistry analysis 48 h post-transfection.

1.6. Subcellular fractionation

Mitochondria from cell lines have been isolated as described by Yang and colleagues [3] with slight modifications. Briefly, wild-type ST7/7Q and mutant ST111/111Q cells were washed twice, harvested in ice cold phosphate-buffered saline (PBS; 140 mM NaCl, 2 mM KCl, 1.5 KH_2PO_4, 8 mM NaH_2PO_4, pH 7.4) and resuspended in isolation buffer (IB; 250 mM sucrose, 20 mM HEPES-KOH pH 7.5, 10 mM KCl, 1.5 mM $MgCl_2$, 1 mM EDTA) with protease and phosphatase inhibitors (0.1 mM phenylmethylsulfonyl fluoride, 1 mM sodium orthovanadate, 10 mg/ml aprotinin and 10 mg/ml leupeptin). Cells were homogenized with a Dounce homogenizer and the suspension was then centrifuged at 800 ×*g* for 10 min at 4 °C to remove nuclei and unbroken cells. The supernatants were centrifuged again at 10,000 ×*g* for 20 min at 4 °C to pellet the heavy membrane fractions containing mitochondria. The pellet fraction was washed, spun down again at 10,000 ×*g*, resuspended in IB containing 1% Triton X-100 and finally saved at −80 °C for later analysis. The cytosolic fraction was obtained as supernatants by further centrifugation at 16,000 ×*g* for 20 min at 4 °C to remove residual mitochondria and saved at −80 °C for later analysis.

1.7. Western blot analysis

Total cellular extracts were collected in lysis buffer containing 50 mM Tris base, pH 7.4, 150 mM NaCl, 2 mM EDTA, 0.1 mM phenylmethylsulfonyl fluoride, 1% NP-40, and supplemented with 1 mM sodium orthovanadate and protease inhibitor mixture (Sigma-Aldrich). Samples were centrifuged at 10,000 ×*g* for 10 min and the protein contents determined by Detergent-Compatible Protein Assay (Bio-Rad, Hercules, CA, USA). For the analysis of the striatum of Hdh mice, heterozygous mutant Hdh7/111Q and wild type Hdh7/7Q mice were killed by cervical dislocation at the age of 8 months. The brain was quickly removed, dissected, frozen in dry ice and stored at −80 °C until use. Protein extraction from striatal tissue and Western blot analysis were performed as previously described [4]. Protein extracts (10–20 μg) were mixed with 5×-SDS sample buffer, boiled for 5 min, resolved on 8–10% SDS-PAGE, and transferred to nitrocellulose membranes (Whatman Schleicher & Schuell, Keene, NH, USA). Blots were blocked in 10% non-fat powdered milk in Tris-buffered saline Tween-20 (TBS-T; 50 mM Tris-HCl, 150 mM NaCl, pH 7.4, 0.05% Tween 20) for 60 min at room temperature. The membranes were then incubated overnight at 4 °C with primary antibodies: Drp1 (DLP1; 1:1000; BD Bioscience, San Jose, CA, USA), phospho-Drp1 (S616) (1:1000, Cell Signaling Technology, Beverly, MA, USA), OPA1 (1:8000, BD Bioscience), Mfn2 (1:2000, Abcam, Cambridge, UK), and Cdk5 J-3 (1:1000, Santa Cruz Biotechnology). Loading control was performed by reproving the membranes with anti-tubulin (1:50,000, Sigma Aldrich) or anti-actin (1:20,000; MP Biochemicals, Irvine, CA, USA) and with anti-OxPhos Complex V (CoxV; 1:3000; Molecular Probes Inc., Eugene, OR, USA) for mitochondrial fractions. The membranes were then rinsed three times with TBS-T and incubated with horseradish peroxidase-conjugated secondary antibody (1:3000; Promega Madison, WI, USA) for 1 h at room temperature. After washing for 30 min with TBS-T, the membranes were developed using the enhanced chemiluminescence ECL kit (Santa Cruz Biotechnology). The intensity of immunoreactive bands was quantified by using Image J software (National Institutes of Health, Bethesda, MD, USA). Data are expressed as the mean ± SEM of band density.

1.8. Immunocytochemistry and confocal analysis

Striatal cells were fixed in 4% paraformaldehyde (Electron Microscopy Science EMS, Hatfield, PA, USA) for 10 min, rinsed in PBS, treated with 0.1 M Glycine for 20 min, and then permeabilized in 0.1% saponin for 10 min. Blocking was done in 1% bovine serum albumin in phosphate-buffered saline for 1 h. Specimens were incubated with primary antibody TOM20 (1:250, Santa Cruz Biotechnology) for 2 h at room temperature. Thereafter, samples were incubated with the following secondary antibodies: AlexaFluo 488 anti-rabbit (1:100; Jackson Immunoresearch, West Grove, PA) and Phalloidin-conjugated with TRITC (1:1000, Sigma Chemicals). Nuclei were stained with the Hoechst 33258 (1:10,000, Molecular Probes, Life Technologies) for 5 min. For detection of D1 receptor on cell surface, the permeabilization with saponin was omitted and samples were incubated with primary antibody anti-Dopamine Receptor D1 (1:500, Abcam) overnight. Afterwards, samples were incubated with the secondary antibody AlexaFluo 488 anti-rabbit (1:100; Jackson Immunoresearch). For immunocytochemical experiments in primary cultures, eight days after plating, neurons were fixed with 4% PFA/phosphate buffer for 10 min, rinsed in PBS, blocked in PBS containing 0.1 M glycine for 10 min and permeabilized in PBS containing 0.1% saponin for 10 min and blocked in PBS containing Normal Horse Serum 15% for 30 min at room temperature. Neurons were then washed in PBS and incubated overnight at 4 °C with primary antibodies TOM20 (1:250, Santa Cruz Biotechnology) and MAP2 (1:500, Sigma-Aldrich) and detected with AlexaFluo 488 anti-rabbit and Cy3 anti-mouse secondary antibodies (1:100, Jackson ImmunoResearch). As negative controls, some neurons were processed as described in the absence of primary antibody and no signal was detected. Nuclei were stained with the Hoechst 33258 (1:10,000, Molecular Probes, Life Technologies) for 5 min. Stained cells and neurons were then washed twice with PBS and mounted under glass coverslips with Mowiol. Immunofluorescence was analyzed by confocal microscopy using a Leica TCS SP5 laser scanning spectral confocal microscope (Leica Microsystems Heidelberg GmbH). Confocal images were taken using a 63× numerical aperture objective with a 3× digital zoom and standard pinhole. For each cell, the entire three-dimensional stack of images from the ventral surface to the top of the cell was obtained by using the Z drive in the Leica TCS SP5 microscope. The size of the optical image was 0.4 μm.

1.9. Analysis of mitochondrial morphology

Quantitative analyses of mitochondrial morphology were performed as previously described [5,6]. Briefly, digital images were processed through a convolve filter to obtain isolated and equalized fluorescent pixels and then to a thresholding step using the NIH-developed ImageJ software (National Institutes of Health, Bethesda, MD). This procedure yields a binary image containing black mitochondrial structures on a white background (Supplementary Fig. 1). From this binary image, individual mitochondria (particles) were subjected to particle analyses to

acquire Form Factor (FF, ($4\pi \times Am/Pm^2$) where Pm is the length of mitochondrial outline and Am is the area of mitochondrion) and Aspect Ratio values (AR, the ratio between the major and minor axis of the ellipse equivalent to the mitochondrion) as well as the number of mitochondria per cell. An AR value of 1 indicates a perfect circle, and as mitochondria elongate and become more elliptical, AR increases. A FF value of 1 corresponds to a circular, unbranched mitochondrion, and higher FF values indicate increase of mitochondrial complexity (length and branching). For determination of the percentage of cells with fragmented mitochondria, a cell was determined to have fragmented mitochondria if it had ≥50% of its mitochondria with length/width (axis) ratios <2.5. In average 25–30 cells/genotype were analyzed from 3 to 6 independent experiments. For the analysis in neurons, the number of mitochondria per micron of axon was measured using NIH ImageJ software.

1.10. Drp1 immunoprecipitation and GTPase enzymatic activity assay

Wild-type ST7/7Q and mutant ST111/111Q cells were washed with cold PBS and incubated on ice in lysis buffer (20 mM Tris [pH 7.5], 0.6% CHAPS, 10% glycerol, 1 mM sodium orthovanadate and protease inhibitor cocktail) for 15 min. Cells were scraped and then disrupted 10 times by repeated aspiration through a 25-gauge needle. Samples were centrifuged at 10,000 ×*g* for 10 min and the supernatant was saved as the whole cell extract. To determine GTPase activity of Drp1, a total of 400 μg of whole-cell extract was immunoprecipitated overnight with 25 μg of anti-Drp1 antibody (BD Bioscience) and 40 μl of protein A/G-agarose (Santa Cruz Biotechnology). For the analysis of Drp1 enzymatic activity in Hdh mice, frozen striatal tissues from heterozygous mutant Hdh7/111Q and wild type Hdh7/7Q mice at the age of 8 months were washed with cold PBS and incubated on ice in lysis buffer (20 mM Tris [pH 7.5], 0,6% CHAPS, 10% glycerol, 1 mM sodium orthovanadate and protease inhibitor cocktail) for 15 min. Tissue was homogenized with a Dounce homogenizer and the lysate was centrifuged at 10,000 ×*g* for 10 min and the supernatant was saved as the whole tissue extract. To determine GTPase activity of Drp1, a total of 400 μg of whole-tissue extract was immunoprecipitated overnight with 25 μg of anti-Drp1 antibody (BD Bioscience) and 40 μl of protein A/G-agarose (Santa Cruz Biotechnology). GTPase activity of the protein was determined using a GTPase assay kit (Novus Biologicals, Littleton, CO, USA) according to manufacturer's instructions. After three washes with lysis buffer and three washes with GTPase buffer (50 mM Tris [pH 7.5], 2.5 mM $MgCl_2$, and 0.02% 2-mercaptoethanol), the beads were incubated with 0.5 mM GTP at 30 °C for 1 h. Drp1 hydrolyzes GTP to GDP and inorganic phosphorous (Pi) and we measured GTPase activity, based on the amount of inorganic phosphorous that the GTP produces. By adding the ColorLock Gold (orange) substrate to the inorganic phosphorous that is generated from GTP, we assessed GTP activity, based on the inorganic complex solution (green). Colorimetric measurements (green) were read in the wavelength range of 650 nm using a Synergy 2 Multi-Mode Microplate Reader (BioTek Instruments, Inc.; Winooski, VT, USA).

1.11. Real-time quantitative RT-PCR

Total RNA was isolated from the wild-type ST7/7Q and mutant knock-in ST111/111Q striatal cell lines using the total RNA isolation Nucleospin RNA II Kit (Macherey-Nagel). Purified RNA (500 ng) was reverse transcribed using the PrimeScript RT Reagent Kit (Perfect Real Time, Takara Biotechnology Inc.). The cDNA synthesis was performed at 37 °C for 15 min and a final step at 85 °C for 5 s in a final volume of 20 μl according to the manufacturer's instructions. The cDNA was then analyzed by quantitative RT-PCR using the following PrimeTime qPCR Assays (Integrated DNA Technologies, Inc.): Dnm1l (Mm.PT.56a.16160059); 18S (Hs.PT.39a.22214856.g) and Actinβ (Mm.PT.39a.22214843.g). RT-PCR was performed in 12 μl of final volume on 96-well plates using the Premix Ex Taq (Probe qPCR) (TAKARA BIOTECHNOLOGY (Dalian) Co., LTD). Reactions included Segment 1:1 cycle of 30 s at 95 °C and Segment 2: 40 cycles of 5 s at 95 °C and 20 s at 60 °C. All quantitative PCR assays were performed in duplicate. To provide negative controls and exclude contamination by genomic DNA, the PrimeScript RTEnzyme was omitted in the cDNA synthesis step. The quantitative PCR data were quantified using the comparative quantitation analysis program of MxProTM quantitative PCR analysis software version 3.0 (Stratagene) using 18S and Actinβ gene expression as housekeeping genes.

1.12. Statistical analysis

All the data were analyzed with the program GraphPad Prism version 5.0a (Graph Pad Software). Results are expressed as mean ± SEM. Unpaired Student's *t*-test for differences between two groups or One-way ANOVA followed by the post hoc Newman–Keuls multiple comparison test were used to assess significance ($p < 0.05$), as indicated in figure legends.

2. Introduction

Huntington's disease (HD) is an autosomal-dominant inherited neurodegenerative disorder, characterized by progressive behavioral, motor and cognitive deficits [7,8]. The predominant neuropathological hallmark of HD is the selective loss of medium spiny neurons within the striatum that extends to other brain regions with the progression of the disease [9]. Although mutant huntingtin (mHtt) represents a key factor in the pathogenesis of the disease, the molecular mechanisms underlying the preferential vulnerability of the striatum to mHtt toxicity remain unclear. From last years, compelling evidence argues in favor of a role of mitochondrial dysfunction in HD neuropathology [10–12]. Thus, the expression of mHtt leads to deficits in energy metabolism [13], alterations in mitochondrial calcium handling [14,15] and severe changes in mitochondrial structure integrity [16,17]. However, given the ubiquitous expression of mHtt within the brain other factors should contribute to alter mitochondrial function in the striatum. One hypothesis is that dopamine (DA), which is present at high concentrations in the striatum compared to other brain areas, might increase the sensitivity of mitochondria to mHtt toxicity inducing mitochondrial dysfunction and neurodegeneration. Actually, by using primary striatal cultures expressing the N-terminal mHtt fragment it has been reported that DA acting via D2 receptors reduces the levels of the mitochondrial Complex II (mCII) increasing the vulnerability of striatal cells to mHtt-induced cell death [18]. Besides D2 receptors, we and others have also demonstrated a critical role for D1 receptors in striatal neurodegeneration in HD [2,19]. Thus, we reported that activation of D1 receptors induces an increase in the susceptibility of mutant huntingtin striatal cells to cell death, an effect that was mediated by Cyclin-dependent kinase-5 (Cdk5) [2]. Importantly, Cdk5 has been identified as an upstream kinase that regulates mitochondrial fission during neuronal apoptosis while its suppression attenuates apoptotic mitochondrial fragmentation [20,21]. In this view, we hypothesized that the increased susceptibility of mutant huntingtin striatal cells to D1R activation could be mediated by Cdk5-induced disturbances in mitochondrial function. To validate this theory we used precise genetic HD models expressing endogenous levels of full-length wild-type or mutant huntingtin [1,2]. Our results reveal a new role for Cdk5 in HD pathology by playing a key role in regulating mitochondrial fission events involved in striatal neurodegeneration and highlight Cdk5 as a therapeutic target to treat mitochondrial dysfunction in HD and other neurodegenerative disorders.

3. Results

3.1. Mutant ST111/111Q striatal cells exhibit aberrant mitochondrial dynamics

Abnormalities in mitochondrial morphology and dynamics have been reported in HD as early pathological events [22–24]. To determine

whether mitochondrial morphology was altered in our HD striatal cell model, wild-type ST7/7Q and mutant ST111/111Q huntingtin striatal cells were stained with TOM20 and phalloidin and mitochondrial population was analyzed by confocal microscopy (Fig. 1A). Morphometric analysis revealed that mutant ST111/111Q striatal cells display significant differences in the mitochondrial morphology compared to wild-type ST7/7Q cells. Thus, the values of the Aspect Ratio (AR) and Form factor (FF) demonstrated reduced mitochondrial length (~10% decrease; $p < 0.05$. Fig. 1B) and lower mitochondrial complexity and decreased branching (~14%; $p < 0.05$. Fig. 1C), respectively. These alterations correlated in mutant cells with a significant increase in the number of mitochondria per cell (~15%; $p < 0.01$. Fig. 1D) Moreover, when the percentage of cell population showing mitochondrial fragmentation was analyzed more than 40% of mutant ST111/111Q striatal cells exhibited fragmented mitochondria whereas only 20% of wild-type ST7/7Q cells showed this mitochondrial fission morphology ($p < 0.01$; Fig. 1E). Altogether, these findings suggest a toxic effect of mHtt on mitochondrial dynamics.

3.2. Mutant huntingtin deregulates the levels and activity of mitochondrial fission/fusion proteins in ST111/111Q striatal cells

Changes in mitochondrial morphology depend on the balance of opposing fission and fusion events [25]. Interestingly, mHtt has been reported to induce changes in the expression of different pro-fission and pro-fusion mitochondrial proteins [26]. To understand the molecular basis of the observed abnormal mitochondrial fragmentation we determined the levels of mitochondria-shaping proteins in our striatal cell lines by Western blot analysis (Fig. 2). No significant differences in the total levels of the fusion protein Opa1 were observed between genotypes (Fig. 2A). However, when the mitochondrial fraction was analyzed, mutant ST111/111Q cells displayed significantly lower levels of Opa1 compared to those in wild-type ST7/7Q cells (20% decrease; $p < 0.05$). Next the levels of another essential fission protein, Mfn2 were investigated. No significant changes either between subcellular fractions or between genotypes were observed (Supplementary Fig. 2). Surprisingly, we also found a significant decrease (30% decrease; $p < 0.05$. Fig. 2B) in the total levels of the fission protein Drp1 in mutant compared to wild-type striatal cells, a reduction that was even higher when mitochondrial subcellular fractions were evaluated (50% decrease; $p < 0.01$) without changes in the cytosolic fraction. To determine if this decrease was due to altered gene transcription, Drp1 mRNA expression was evaluated. A statistically significant decrease in Drp1 mRNA levels was detected in mutant ST111/111Q compared to wild-type ST7/7Q striatal cells (20% decrease; $p < 0.05$. Fig. 2C) suggesting an involvement of mHtt in the transcriptional deregulation of Drp1. Since mHtt abnormally interacts with Drp1 altering its structure and increasing its enzymatic activity [27], we then evaluated Drp1-GTPase activity in striatal cells (Fig. 2D). Despite the low levels of Drp1 expression found in mutant huntingtin cells, a significant increase (~3.5-fold increase; $p < 0.01$. Fig. 2D) in the GTP-binding activity of Drp1 was observed in mutant compared to wild-type cells suggesting that enhanced mitochondrial fragmentation in mutant huntingtin cells could be related with higher Drp1 activity.

3.3. Hdh7/111Q knock-in mutant mice display impaired mitochondrial dynamics and increased Drp1 activity

To extend our mitochondrial findings in an in vivo HD model, we next analyzed whether alterations in mitochondrial dynamics were also detected in primary striatal neurons from Hdh7/111Q knock-in mutant mice. Confocal microscopy analysis (Fig. 3A) revealed that mitochondria from mutant Hdh7/111Q primary striatal neurons were more fragmented with respect to those in wild-type Hdh7/7Q mice (~30%; $p < 0.05$. Fig. 3B). Considering that abnormalities in the morphology and function of mitochondria persist along the disease progression

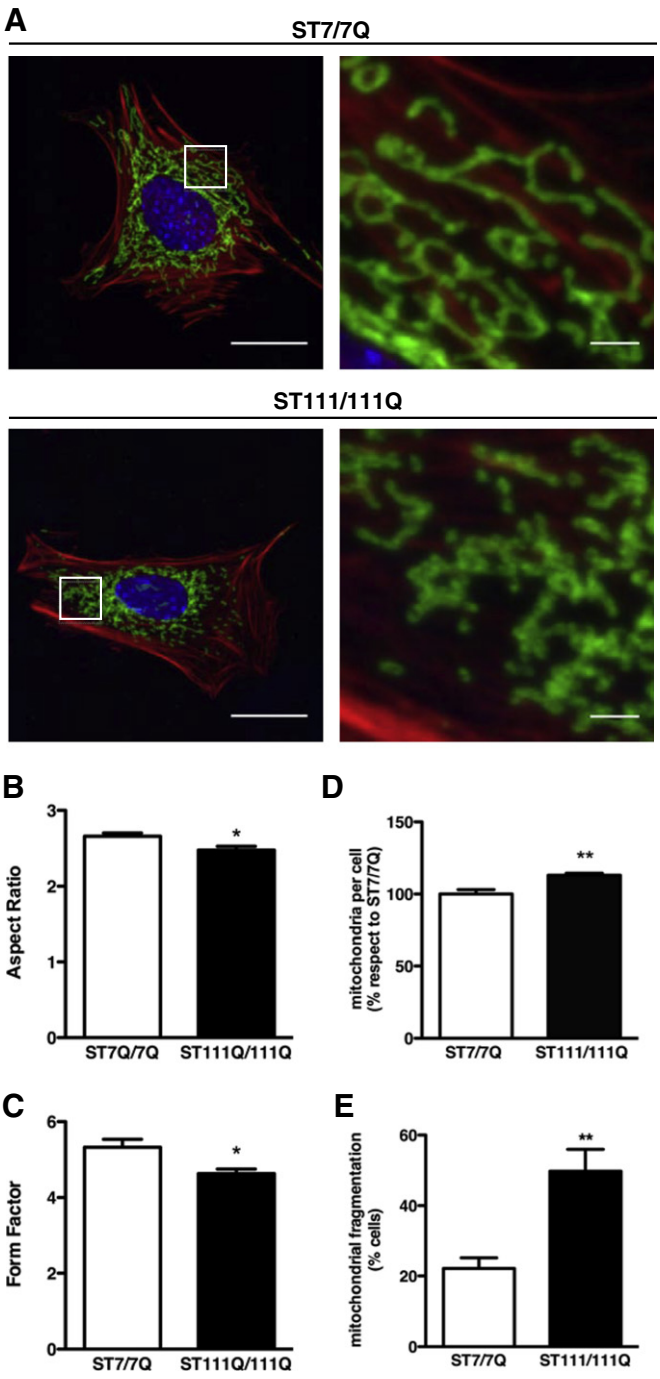

Fig. 1. ST111/111Q mutant cells show increased mitochondrial fragmentation. (A) Representative confocal images showing mitochondrial morphology in wild-type ST7/7Q and mutant ST111/111Q cells immunostained with anti-TOM20 (green), anti-Phalloidin-TRITC (red) and Hoechst stain (blue); scale bar 20 μm. The boxed areas are enlarged in the panels on the right; scale bar 2 μm. (B, C) Bar histogram showing the Aspect Ratio (AR) and Form Factor (FF) value. *$p < 0.05$ as determined by unpaired Student's *t*-test. (D) Bar histogram showing the number of mitochondria per cell. *$p < 0.05$ as determined by unpaired Student's *t*-test. (E) Bar histogram showing the percentage of cells with fragmented mitochondria relative to the total number of cells. **$p < 0.01$ as determined by unpaired Student's *t*-test. Data represent mean ± SEM of 6 independent experiments in which 25–30 cells/genotype were analyzed with ImageJ software.

[17], alterations in the levels of the fission protein Drp1 were analyzed in the striatum of Hdh7/111Q knock-in mutant mice at 8 months of age. Immunoblot analysis revealed no changes in striatal Drp1 protein

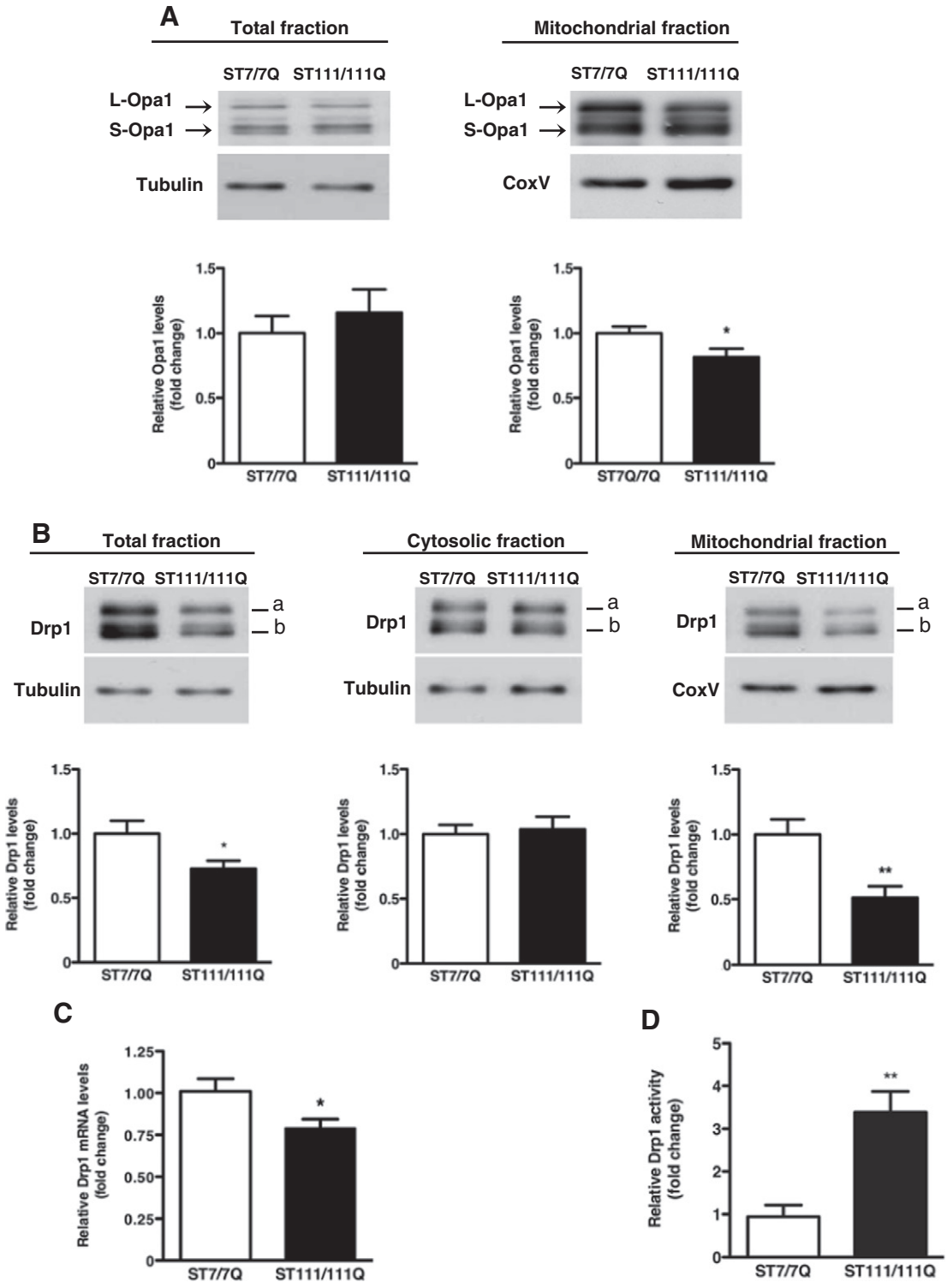

Fig. 2. ST111/111Q mutant cells exhibit altered expression, subcellular distribution and activity of Drp1. (A, B) Representative Western blots showing the levels of the fusion protein Opa1 in total and mitochondrial fractions and the fission protein Drp1 in total, cytosolic and mitochondrial fractions from wild-type ST7/7Q and mutant ST111/111Q cells. α-Tubulin (total and cytosol) or CoxV (mitochondria) were used as loading controls. Letters confer to the different isoforms recognized by the respective antibodies (L-Opa1 and S-Opa-1; DRP1: a–b). Bar histograms indicate the relative fold change ± SEM of 9 independent experiments; $^{**}p < 0.01$, $^{*}p < 0.05$ vs. wild-type ST7/7Q cells as determined by unpaired Student's *t*-test. (C) Histogram showing Drp1 mRNA expression analyzed by RT-PCR in wild-type ST7/7Q and mutant ST111/111Q cells. Data were normalized to 18S and actinβ gene expression. Bar histogram represents the relative fold change ± SEM of 7 independent experiments. $^{*}p < 0.05$ vs. wild-type ST7/7Q cells as determined by unpaired Student's *t*-test. (D) Histogram showing GTPase Drp1 enzymatic activity in striatal extracts obtained from wild-type ST7/7Q and mutant ST111/111Q cells. Bar diagram represents the relative fold change ± SEM of 5 independent experiments. $^{**}p < 0.01$ vs. wild-type ST7/7Q cells as determined by unpaired Student's *t*-test.

levels between mutant Hdh7/111Q and wild-type Hdh7/7Q mice in any of the subcellular fractions analyzed (Fig. 3C). However and in agreement with our results in mutant ST111/111Q striatal cells, the enzymatic activity of Drp1 was significantly increased (~2-fold increase; $p < 0.05$. Fig. 3D) in mutant Hdh7/111Q mice compared to wild-type Hdh7/7Q mice. These data support the idea that

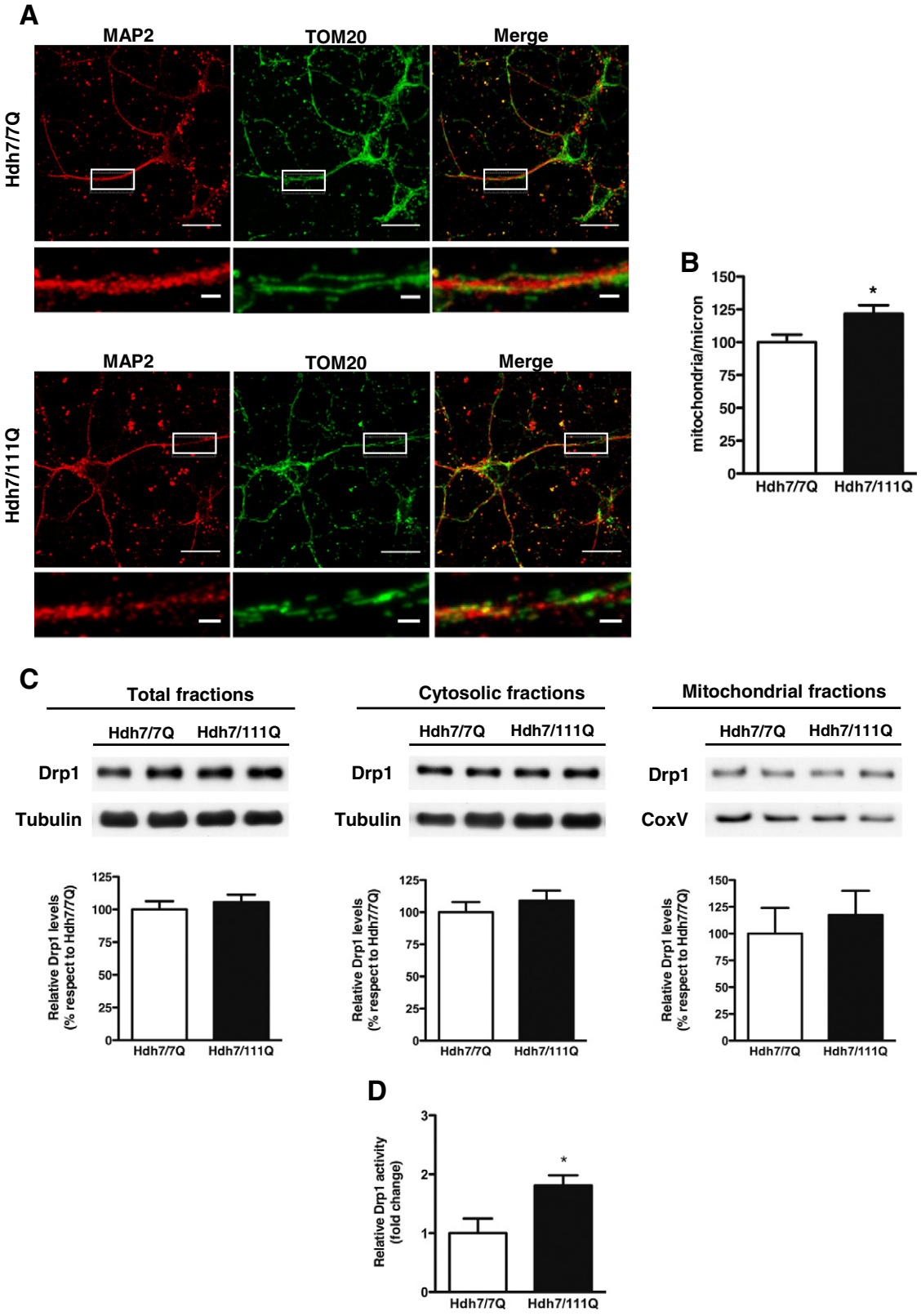

Fig. 3. Mutant Hdh7/111Q mice exhibit impaired mitochondrial fragmentation associated with increased Drp1 activity. (A, B) Representative confocal images of striatal primary culture from wild-type Hdh7/7Q and mutant Hdh7/111Q mice immunostained with anti-TOM20 (green) and anti-MAP2 (red); scale bar 20 μm. The boxed areas are enlarged in the panels on the bottom; scale bar 4 μm. The bar graph provides the percentage of mitochondria per axonal micron. Data represent mean ± SEM of 4 independent experiments in which 20 neurons/genotype were analyzed with ImageJ software; *$p < 0.05$ vs. wild-type Hdh7/7Q mice as determined by unpaired Student's *t*-test. (C) Representative Western blots showing the levels of the fission protein Drp1 in total, cytosolic and mitochondrial fractions obtained from the striatum of wild-type Hdh7/7Q and mutant Hdh7/111Q mice. α-Tubulin (total and cytosol) or CoxV (mitochondria) were used as loading controls. Bar histograms indicate the relative levels of Drp1 ± SEM of 7 independent experiments. (D) Histogram showing GTPase Drp1 enzymatic activity in striatal extracts obtained from 8-month-old wild-type Hdh7/7Q and mutant Hdh7/111Q mice. Bar histogram indicates the relative fold change ± SEM of 6 independent experiments; *$p < 0.05$ vs. Hdh7/7Q as determined by unpaired Student's *t*-test.

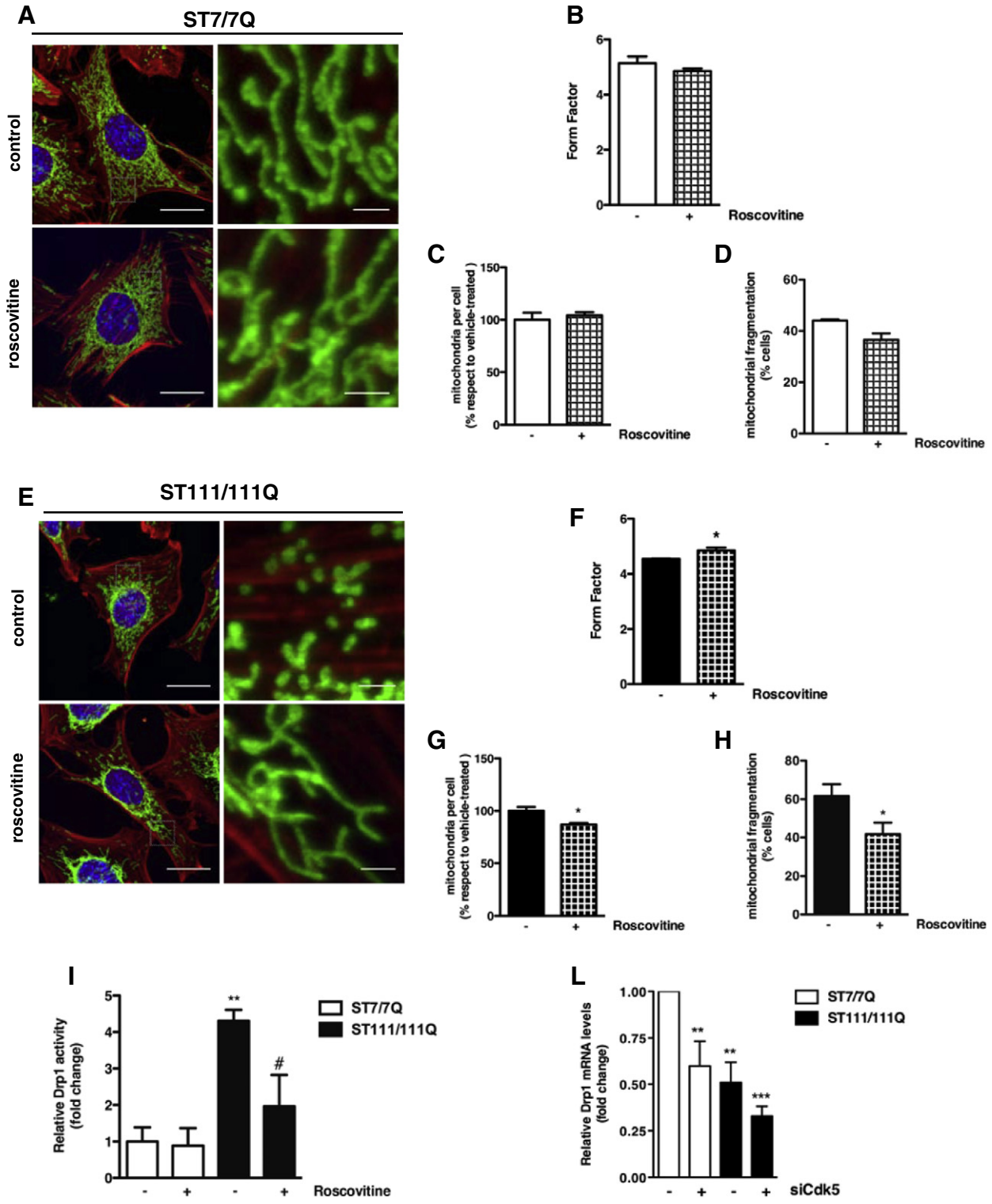

Fig. 4. Aberrant Cdk5 activity in ST111/111Q mutant cells induces mitochondrial fragmentation. (A, E) Representative confocal images showing mitochondrial morphology in wild-type ST7/7Q and mutant ST111/111Q cells treated with roscovitine (20 μM). Cells were stained with anti-TOM20 (green), anti-Phalloidin-TRITC (red) and Hoechst stain (blue); scale bar 20 μm. Panels on the right show enlargement of the boxed areas; scale bar 2 μm. Bar histograms showing: (B, F) the relative Form Factor (FF) value, (C, G) the percentage of number of mitochondria per cell and (D, H) the percentage of cells with fragmented mitochondria relative to the total number of cells. Data represent mean ± SEM of 5 independent experiments in which 25–30 cells/condition were analyzed with ImageJ software. *$p < 0.05$ vs. vehicle treated condition as determined by unpaired Student's *t*-test. (I) Histogram showing GTPase Drp1 enzymatic activity in striatal extracts obtained from vehicle or roscovitine treated wild-type ST7/7Q and mutant ST111/111Q cells. Bar histogram indicates the relative fold change ± SEM of 4 independent experiments; **$p < 0.01$ vs. wild-type ST7/7Q cells and $^{\#}p < 0.05$ vs. vehicle-treated ST111/111Q cells as determined by One-way ANOVA with Newman–Keuls post hoc analysis. (L) Histogram showing Drp1 mRNA expression analyzed by RT-PCR in wild-type ST7/7Q and mutant ST111/111Q cells transfected with siRNA or siCdk5. Data were normalized to 18S and actinβ gene expression. Bar histogram indicates the relative fold change ± SEM of 7 independent experiments. ***$p < 0.001$ and **$p < 0.01$ vs. siRNA transfected ST7/7Q cells as determined by One-way ANOVA with Newman–Keuls post hoc analysis.

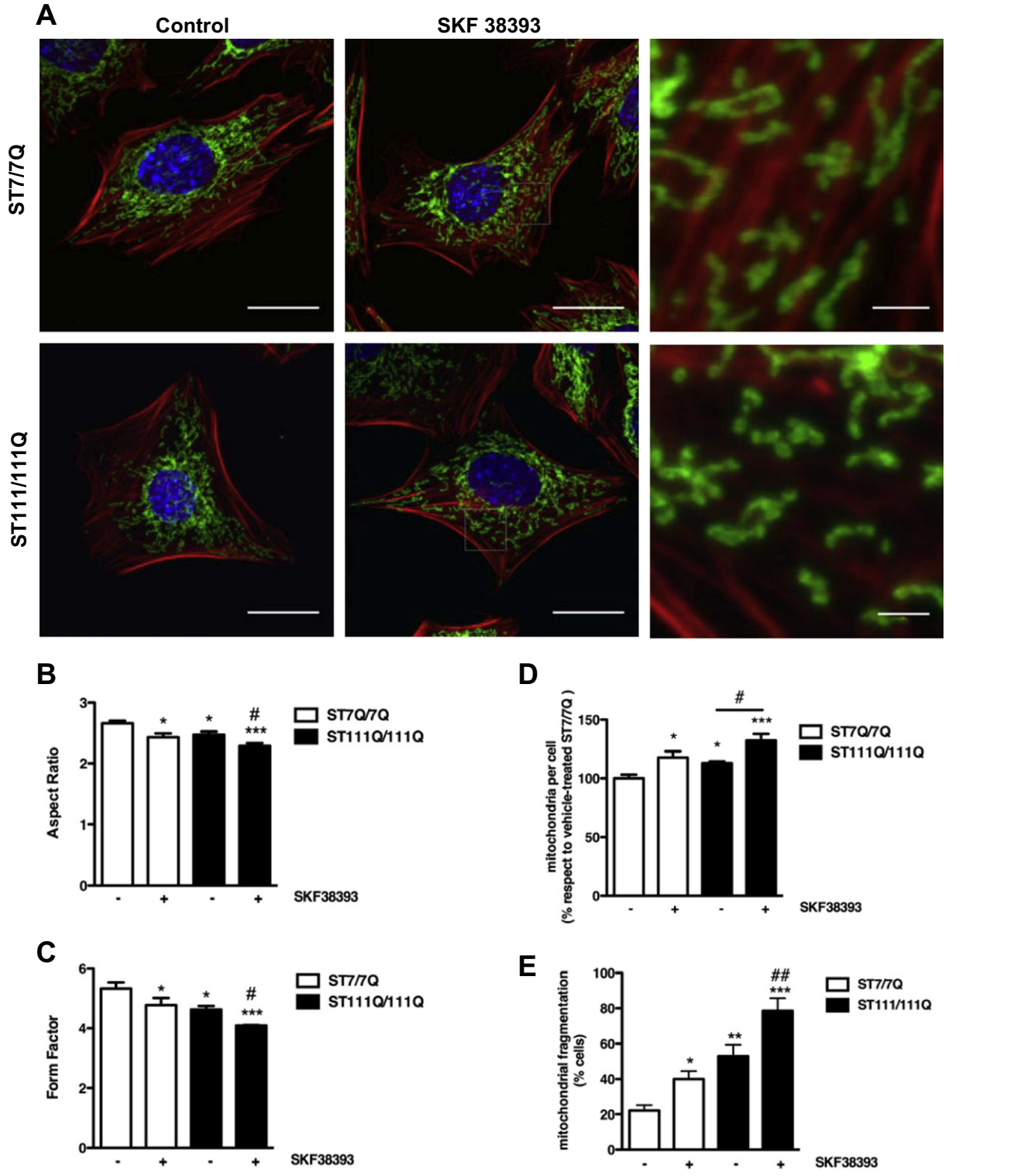

Fig. 5. Dopaminergic D1 receptor activation increases mitochondrial fission events and mitochondrial branching defects in striatal cells. (A) Representative confocal images showing mitochondrial morphology in wild-type ST7/7Q and mutant ST111/111Q cells treated with vehicle or the dopaminergic agonist SKF 38393 (60 μM). Cells were stained with anti-TOM20 (green), anti-Phalloidin-TRITC (red) and Hoechst stain (blue); scale bar 20 μm. Last panels on the right show enlargement of the boxed areas; scale bar 2 μm. (B, C) Bar histograms showing mitochondrial size by Aspect Ratio (AR) values and mitochondrial branching changes determined by the analysis of the Form Factor (FF) value in SKF 38393-treated and vehicle-treated wild-type ST7/7Q and mutant ST111/111Q cells. Data represent mean ± SEM of 6 independent experiments in which 25–30 cells/condition were analyzed with ImageJ software. $^{***}p < 0.001$, $^{*}p < 0.05$ vs. vehicle-treated ST7/7Q cells and $^{\#}p < 0.05$ vs. vehicle-treated ST111/111Q cells as determined by One-way ANOVA with Newman–Keuls post hoc analysis. (D) Bar histogram showing percentage of number of mitochondria per cell. (E) Bar histogram showing the percentage of vehicle or SKF 38393-treated wild-type ST7/7Q and mutant ST111/111Q cells with fragmented mitochondria relative to the total number of cells. Data represent mean ± SEM of 6 independent experiments in which 25–30 cells/condition were analyzed with ImageJ software. $^{***}p < 0.001$, $^{**}p < 0.01$ and $^{*}p < 0.05$ vs. vehicle-treated ST7/7Q cells and $^{\#\#}p < 0.01$ and $^{\#}p < 0.05$ vs. vehicle-treated ST111/111Q cells as determined by one-way ANOVA with Newman–Keuls post hoc analysis.

mitochondrial abnormalities in HD models are related with enhanced Drp1 enzymatic activity induced by mHtt.

3.4. Cdk5 contributes to Drp1-induced mitochondrial dysfunction in mutant ST111/111Q striatal cells

Cdk5 may promote mitochondrial dysfunction [28] acting as an upstream regulator of mitochondrial fission during neuronal apoptosis [21]. Since we have previously demonstrated an aberrant increase in Cdk5 activity in mutant ST111/111Q cells [2] we next aimed to determine the relevance of Cdk5 in mitochondrial fission. Wild-type ST7/7Q (Fig. 4A) and mutant ST111/111Q cells (Fig. 4E) were treated with the Cdk5 inhibitor roscovitine and mitochondrial morphology was analyzed by confocal microscopy. Roscovitine treatment significantly improved mitochondrial tubular network defects (~10% increase in the Form Factor value; $p < 0.05$. Fig. 4F) and reduced

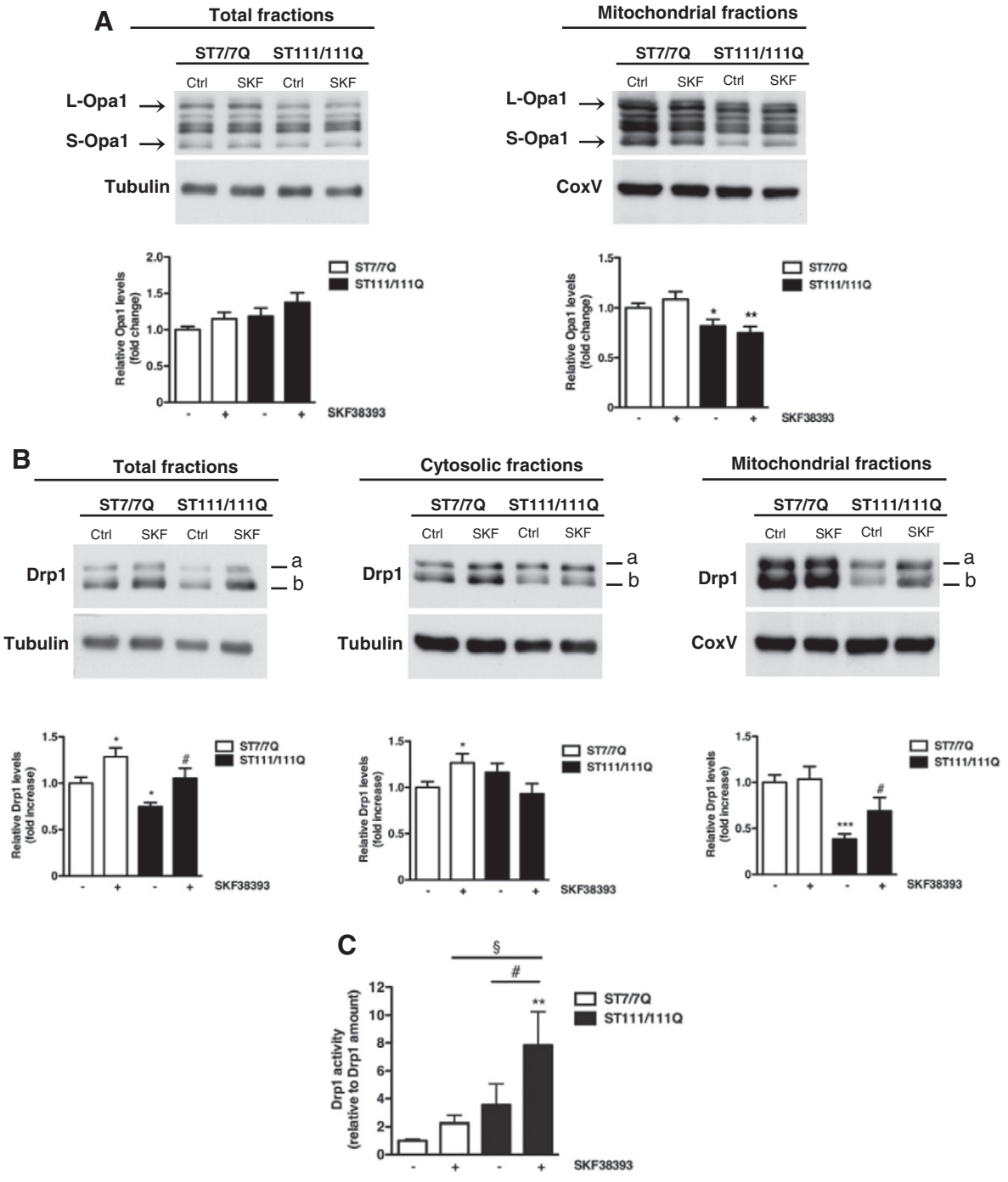

Fig. 6. Aberrant mitochondrial Drp1 activity exacerbates D1R-induced mitochondrial fission in ST111/111Q mutant cells. (A, B) Representative Western blots showing the levels of the fusion protein Opa1 in total and mitochondrial fractions and the fission protein Drp1 in total, cytosolic and mitochondrial fractions obtained from vehicle and SKF 38393 (60 μM) treated wild-type ST7/7Q and mutant ST111/111Q cells. α-Tubulin (total and cytosol) or CoxV (mitochondria) were used as loading controls. Letters indicate the different isoforms recognized by the respective antibodies (L-Opa1 and S-Opa-1; DRP1: a–b). Bar histograms indicate the relative fold change ± SEM of 12 independent experiments. $^{***}p < 0.001$, $^{**}p < 0.01$, $^{*}p < 0.05$ vs. vehicle-treated ST7/7Q cells and $^{\#}p < 0.05$ vs. vehicle-treated ST111/111Q cells as determined by One-way ANOVA with Newman–Keuls post hoc analysis. (C) Histogram showing GTPase Drp1 enzymatic activity in striatal extracts obtained from vehicle or SKF 38393-treated mutant ST111/111Q striatal cells. Bar histogram represents the relative fold change ± SEM of 6 independent experiments; $^{**}p < 0.01$ vs. vehicle-treated ST7/7Q cells, $^{\#}p < 0.05$ vs. vehicle treated ST111/111Q cells and $^{\S}p < 0.05$ vs. SKF 38393 treated ST7/7Q cells as determined by One-way ANOVA with Newman–Keuls post hoc analysis.

mitochondrial fragmentation (~20%; $p < 0.05$. Fig. 4G and H) in mutant but not wild-type huntingtin cells (Fig. 4A–D) suggesting an important role of Cdk5 in mitochondrial dysfunction in HD striatal cells. Since we have demonstrated increased Drp1 activity in mutant huntingtin striatal cells, we next addressed whether the improvement in mitochondrial fragmentation following roscovitine treatment was associated with a reduction in Drp1 activity. According to a role of Cdk5 in mitochondrial impairments, pharmacological inhibition of Cdk5 significantly reduced (~50% decrease; $p < 0.01$. Fig. 4I) Drp1 activity in mutant ST111/111Q cells without any effect in wild-type ST7/7Q cells. Interestingly, we also found that in addition to Drp1 activity Drp1 gene transcription was also modulated by Cdk5. Thus, a significant decrease in Drp1 mRNA expression was observed in wild-type (~40% decrease; $p < 0.01$) and mutant (~70% decrease; $p < 0.001$) huntingtin striatal cells when expression of Cdk5 was reduced by Cdk5 siRNAs (Fig. 4L) revealing a critical role for Cdk5 as a transcriptional regulator of Drp1.

3.5. Activation of dopaminergic D1 receptors increases mitochondrial dysfunction in mutant ST111/111Q striatal cells

We have previously demonstrated that mutant ST111/111Q cells are more susceptible to cell death induced by D1R activation than wild-type ST7/7Q cells [2]. Interestingly, it has been reported that dopamine could negatively influence mitochondrial function [29,30]. Therefore, to determine whether the enhanced vulnerability of mutant ST111/111Q cells to dopamine-induced cell death was mediated by mitochondrial impairments wild-type ST7/7Q and mutant ST111/111Q cells were treated with the D1 receptor agonist SKF 38393 (60 μM) and mitochondrial morphology was analyzed by confocal microscopy (Fig. 5A). First, we analyze whether these striatal cells properly express D1R at the plasma membrane (Supplementary Fig. 3). Cell surface D1R expression examined with an antibody against the extracellular domain of D1R in non-permeable cell conditions was similar between wild type and mutant huntingtin striatal cells. Then mitochondrial fission was examined. Our findings demonstrated that mitochondrial fragmentation occurs quickly in response to D1 receptor activation leading to a significant decrease in the size (Fig. 5B) and mitochondrial reticular network distribution (Fig. 5C) in both cell genotypes. It is important to notice that dopaminergic stimulation was able to further decrease FF and AR values in mutant huntingtin cells compared to vehicle conditions (~10%; $p < 0.05$). The alterations in mitochondrial morphology induced by SKF 38393 treatment were also detected by an increase in the number of organelles per cell (Fig. 5D) showing both genotypes an increment of 20% ($p < 0.05$; Fig. 5E) compared to vehicle conditions. Finally, when the percentage of cells with mitochondrial fragmentation was analyzed, we found that, in wild-type cells D1R activation raised the percentage from 20% to 40% ($p < 0.05$ Fig. 5E) while the transition in mutant cells was from 50% to 80% ($p < 0.01$). These mitochondrial alterations were dose-dependent since the treatment with lower concentration of SKF 38393 (30 μM) did not alter mitochondrial conformation in both cell types (Supplementary Fig. 4). Finally, to validate that SKF 38393 effects on mitochondria morphology were D1R-dependent, wild-type and mutant huntingtin striatal cells were treated with the D1R antagonist SCH 23390 prior to D1R activation and mitochondrial fission was analyzed (Supplementary Fig. 5). Importantly, co-incubation with SCH 23390 completely abrogates SKF 38393-induced alterations in mitochondrial morphology in both cell genotypes. Overall these results indicate that the increased susceptibility of mutant huntingtin striatal cells to dopaminergic activation could be mediated by alterations in the distribution and morphology of the mitochondrial population.

3.6. Activation of dopaminergic D1 receptors alters the levels, distribution and activity of the fission protein Drp1 in ST111/111Q striatal cells

Confocal microscopy analysis has shown that SKF 38393 treatment induces higher mitochondrial fragmentation in mutant compared to wild-type huntingtin cells. To correlate this morphological alterations with changes in mitochondrial fission/fusion proteins, the levels of Opa1 and Drp1 were analyzed in total, cytosolic and mitochondrial fractions obtained from vehicle and SKF 38393 treated wild-type and mutant huntingtin striatal cells. SKF 38393 treatment did not affect the expression of the pro-fusion protein Opa1 neither in wild-type nor in mutant huntingtin striatal cells (Fig. 6A) but induced a significant increase in total Drp1 levels (~1.3-fold increase and ~1.5-fold increase, respectively; $p < 0.05$. Fig. 6B). Interestingly, the distribution of Drp1 within the subcellular compartments following dopaminergic activation was different between cell genotypes. Whereas in wild-type cells the increase in Drp1 levels was found in the cytosolic fraction, that in mutant huntingtin cells was located in the mitochondrial fraction. Given the requirement of Drp1 translocation to the mitochondria for the fission of this organelle [31,32], the aberrant distribution of Drp1 in mutant huntingtin striatal cells may explain the increased mitochondrial fragmentation observed in these cells compared to wild-type cells. Next, we investigated whether dopaminergic stimuli could also affect Drp1 enzymatic activity. An increasing trend, although not significant, in Drp1 activity was found in wild-type cells after SKF 38393 treatment (Fig. 6C). By contrast, a significant increase (~8-fold increase; $p < 0.01$. Fig. 6C) was detected in SKF 38393-treated mutant huntingtin cells suggesting that D1 receptor activation exacerbates Drp1-dependent mitochondrial fission events in ST111/111Q mutant cells.

3.7. Inhibition of Cdk5 prevents D1R-induced mitochondrial fission and mitochondrial branching alterations in striatal cells

We have shown that Cdk5 contributes to mitochondrial fragmentation in mutant ST111/111Q cells while D1R activation increases mitochondrial fission. Interestingly, we have previously reported [2] that aberrant Cdk5 activity mediates D1R-induced neurotoxicity in mutant ST111/111Q striatal cells. Altogether, it prompted us to investigate whether Cdk5 was also mediating the mitochondrial dysfunction induced by dopaminergic D1R activation. To this aim, wild-type and mutant huntingtin striatal cells were treated with roscovitine prior to incubation with SKF 38393 and mitochondrial morphology was analyzed by confocal microscopy (Fig. 7A and E). Roscovitine treatment completely recovered SKF 38393-induced mitochondrial branching alterations (Fig. 7B and F) and prevented mitochondrial fragmentation, either mitochondrial number (Fig. 7C and G) or percentage of cells with mitochondria fragmentation (Fig. 7D and H) in both cell genotypes, pointing Cdk5 as a mediator of D1R-induced mitochondrial fission. To further corroborate these results, Cdk5 protein levels were knocked-down in wild-type and mutant huntingtin striatal cells by using specific Cdk5 siRNAs and mitochondria fragmentation was analyzed following D1R activation (Fig. 8A and E). First, the efficiency of the Cdk5 siRNA to knock-down Cdk5 levels was determined by Western blot analysis. A similar and a significant decrease in Cdk5 levels was found in Cdk5 siRNA transfected cells compared to those transfected with scramble siRNA (~50% decrease; $p < 0.01$. Supplementary Fig. 6). Then, mitochondrial fission was analyzed. Genetic knock-down of Cdk5 completely prevented the decrease in mitochondrial branching (Fig. 8B and F) and the increase in mitochondrial fragmentation induced by SKF 38393 treatment in both wild-type ST7/7Q and mutant ST111/111Q huntingtin striatal cells (Fig. 8C, D, G and H), strongly supporting a role for Cdk5 in D1R-induced mitochondrial dysfunction in striatal cells.

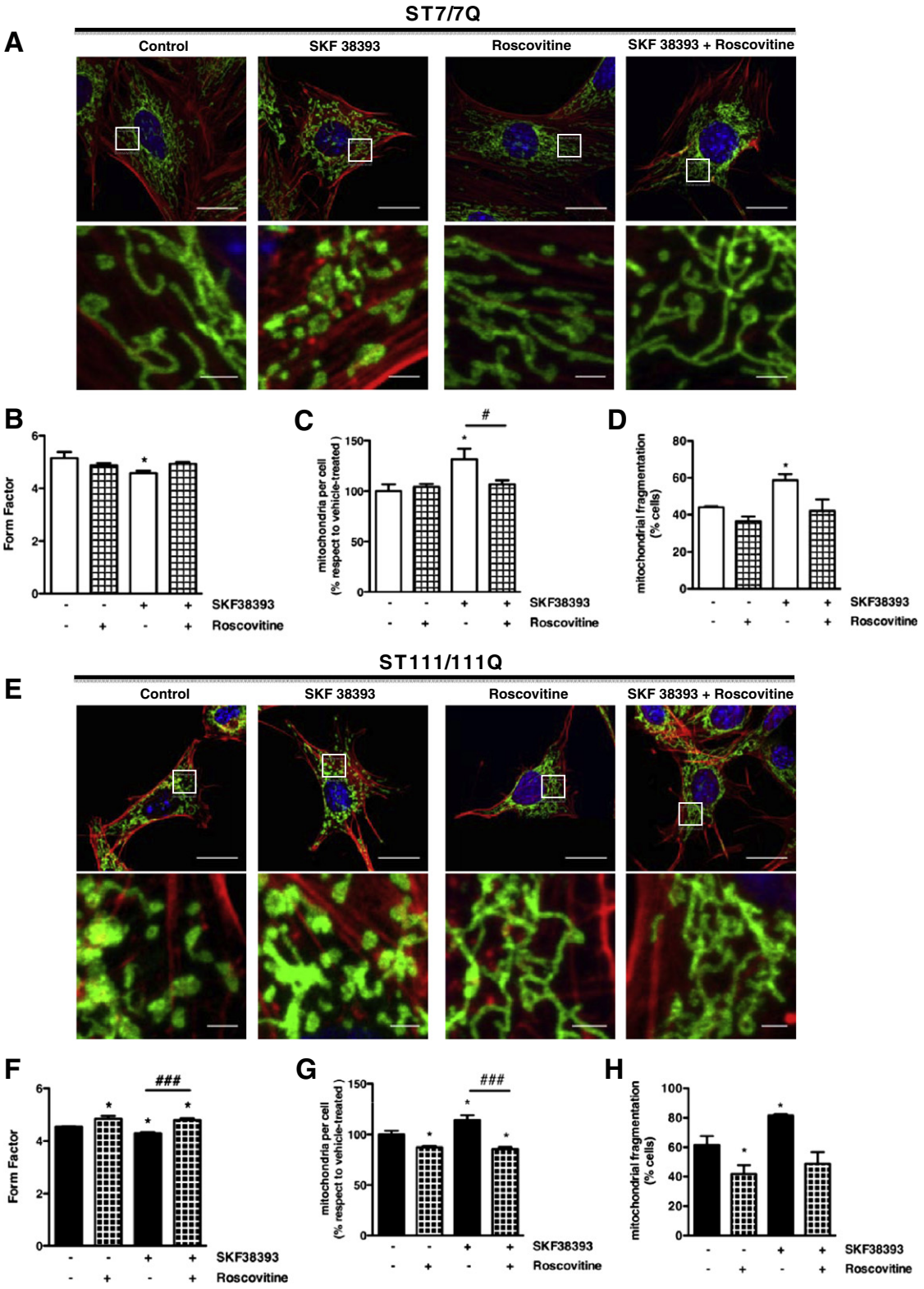

Fig. 7. Cdk5 inhibition restores the mitochondrial network in SKF 38393 treated ST7/7Q wild-type and ST111/111Q mutant cells. (A, E) Representative confocal images showing the mitochondrial morphology in wild-type ST7/7Q and mutant ST111/111Q cells treated with vehicle, SKF 38393 (60 μM), roscovitine (20 μM) or roscovitine + SKF 38393. Cells were stained with anti-TOM20 (green), anti-phalloidin-TRITC (red) and Hoechst stain (blue); scale bar 20 μm. Bottom panels show enlargement of the boxed areas; scale bar 2 μm. (B and F) Bar histogram showing mitochondrial branching changes determined by the analysis of the Form Factor (FF) value in vehicle or treated wild-type ST7/7Q and mutant ST111/111Q cells. Data represent mean ± SEM of 5 independent experiments in which 25–30 cells/condition were analyzed with ImageJ software. $^{*}p < 0.05$ vs. vehicle-treated striatal cells and $^{###}p < 0.001$ vs. SKF 38393 treated cells as determined by One-way ANOVA with Newman–Keuls post hoc analysis. (C and G) Bar histograms showing the percentage of number of mitochondria per cell. Data represent mean ± SEM of 5 independent experiments in which 25–30 cells/condition were analyzed with ImageJ software. $^{*}p < 0.05$ vs. vehicle-treated striatal cells and $^{###}p < 0.001$ and $^{\#}p < 0.05$ vs. SKF 38393 treated cells as determined by One-way ANOVA with Newman–Keuls post hoc analysis. (D and H) Bar histograms showing the percentage of vehicle or treated wild-type ST7/7Q and mutant ST111/111Q cells with fragmented mitochondria relative to the total number of cells. Data represent mean ± SEM of 5 independent experiments in which 25–30 cells/condition were analyzed with ImageJ software. $^{*}p < 0.05$ vs. vehicle-treated striatal cells as determined by One-way ANOVA with Newman–Keuls post hoc analysis.

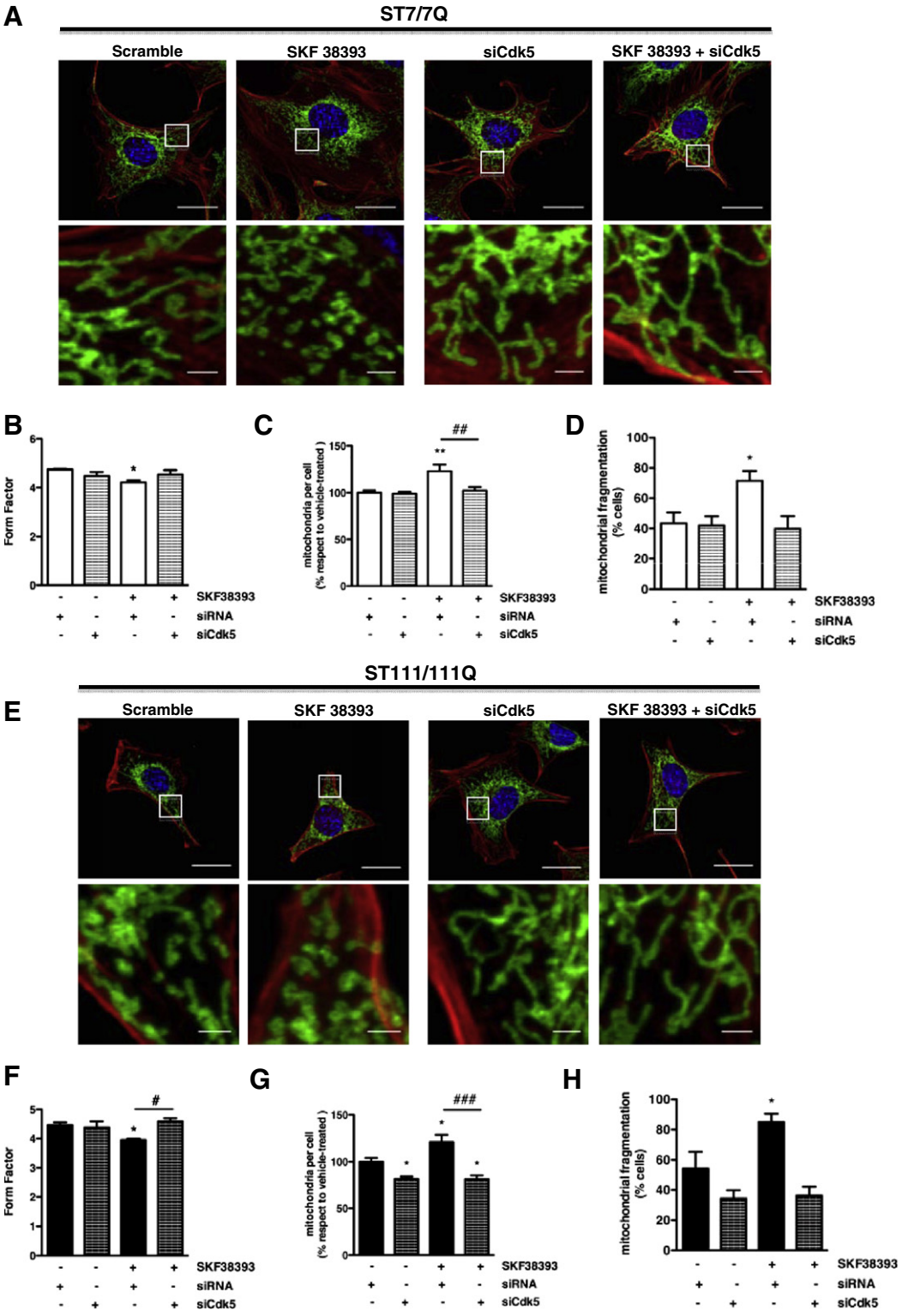

Fig. 8. Inhibition of Cdk5 by Cdk5 siRNA prevents aberrant mitochondrial fission and altered branching induced by D1R activation in ST7/7Q wild-type and ST111/111Q mutant striatal cells. (A and E) Representative confocal images showing the mitochondrial morphology in wild-type ST7/7Q and mutant ST111/111Q cells treated with vehicle or SKF 38393 (60 μM) and transfected with siRNA or siCdk5 RNA. Cells were stained with anti-TOM20 (green), anti-Phalloidin-TRITC (red) and Hoechst stain (blue); scale bar 20 μm. Bottom panels show enlargement of the boxed areas; scale bar 2 μm. (B and F) Bar histogram showing mitochondrial branching changes determined by the analysis of the Form Factor (FF) value in vehicle or SKF 38393 treated wild-type ST7/7Q and mutant ST111/111Q cells. Data represent mean ± SEM of 5 independent experiments in which 25–30 cells/condition were analyzed with ImageJ software. $^{*}p < 0.05$ vs. vehicle-treated siRNA-transfected striatal cells and $^{\#}p < 0.05$ vs. SKF 38393-treated siRNA-transfected cells as determined by One-way ANOVA with Newman–Keuls post hoc analysis. (C and G) Bar histograms showing the percentage of number of mitochondria per cell. Data represent mean ± SEM of 5 independent experiments in which 25–30 cells/condition were analyzed with ImageJ software. $^{**}p < 0.01$ and $^{*}p < 0.05$ vs. vehicle-treated siRNA-transfected striatal cells and $^{\#\#\#}p < 0.001$ and $^{\#\#}p < 0.01$ vs. SKF 38393-treated siRNA-transfected cells as determined by One-way ANOVA with Newman–Keuls post hoc analysis. (D and H) Bar histograms showing the percentage of vehicle or SKF 38393 treated wild-type ST7/7Q and mutant ST111/111Q cells with fragmented mitochondria relative to the total number of cells. Data represent mean ± SEM of 5 independent experiments in which 25–30 cells/condition were analyzed with ImageJ software. $^{*}p < 0.05$ vs. vehicle-treated striatal cells as determined by One-way ANOVA with Newman–Keuls post hoc analysis.

3.8. Inhibition of Cdk5 abrogates the D1R-induced increase and the mitochondrial translocation of Drp1 in ST111/111Q striatal cells

We have demonstrated that mitochondrial fragmentation induced by D1R activation was prevented by down-regulation of Cdk5 while activation of D1R induced an increase in the levels of the fission protein Drp1. Hence, we analyzed whether mitochondrial fission induced by D1R activation was mediated by a Cdk5-dependent increase in Drp1 function. Wild-type ST7/7Q and mutant ST111/111Q cells were transfected with scramble or Cdk5 siRNA, treated with vehicle or SKF 38393 and levels of Drp1 were determined by Western blot analysis (Fig. 9A). We found that reduction of Cdk5 expression prevented the abnormal increase of Drp1 caused by dopaminergic activation in both cell genotypes (Fig. 9B). Since we previously demonstrated in mutant huntingtin cells (Fig. 6) that D1R activation induces an increase in mitochondrial Drp1, we evaluated whether aberrant Cdk5 activity could be responsible of SKF 38393-induced Drp1 mitochondrial enrichment. Consistent with this idea, we found that mitochondrial Drp1 accumulation in mutant huntingtin striatal cells was completely prevented by inhibition of Cdk5 with roscovitine (Fig. 9C), suggesting that Cdk5 mediates D1 receptor-induced mitochondrial fragmentation by modulation of Drp1 protein levels and distribution.

4. Discussion

Mitochondria are essential organelles for neuronal function and survival given the prominent dependence of neuronal cells on mitochondrial ATP production to support different functions including membrane potential maintenance, neurotransmitter release and uptake or transportation of synaptic vesicles [33]. In HD the most important neuropathological alteration is the preferential loss of medium spiny neurons within the striatum [9]. Though the precise molecular mechanisms leading to this specific cell death are unknown, growing evidence have emerged for impaired mitochondrial function as a causative factor [34,35]. In this view, here, we have reported in a precise genetic HD striatal cell line and in HD striatal cell cultures impaired mitochondrial dynamics manifested as higher mitochondrial fragmentation and decreased mitochondrial branching compared to wild-type striatal cells, which is consistent with previous studies reporting, in different HD models, altered levels of fission/fusion proteins and increased mitochondrial fission [17,24,36]. Surprisingly, enhanced mitochondrial fragmentation in mutant huntingtin striatal cells was not associated with an increase in the levels of the fission protein Drp1, neither at the total nor at the mitochondrial level, but with a decrease. Importantly, the decrease in Drp1 protein levels in mutant huntingtin cells was associated with lower Drp1 mRNA expression suggesting that mHtt may alter mitochondrial dynamics by acting on transcriptional regulation of Drp1. In this view, it has been described that p53 is an important modulator of mitochondrial fission by transcriptional regulation of Drp1 expression [37]. Interestingly, previous works have demonstrated reduced p53-mediated gene transcription in mutant huntingtin expressing cells suggesting that the decrease in Drp1 mRNA levels found in mutant striatal cells could be related with a deficient p53 transcriptional function [38].

If the levels and expression of Drp1 are low in mutant huntingtin striatal cells, one intriguing question is how mitochondrial fragmentation can be enhanced in these cells. Interestingly, we found that the GTPase activity of Drp1, that is critical for mitochondrial fragmentation, was significantly higher in mutant huntingtin striatal cell lines and in the striatum of HD knock-in mutant mice indicating that in the presence of mHtt, the activity of Drp1 is aberrantly activated. These findings are in agreement with previous studies showing elevated Drp1 activity in the striatum and cortex of BACHD mice and in the cortex of HD patients [39]. Importantly, besides an increase in Drp1 activity a decrease in the levels of the fusion protein Opa1 was also observed suggesting altogether, that an imbalance in the levels and activity of proteins involved in the mitochondrial dynamic machinery could be responsible for the abnormal mitochondrial morphology observed in mutant huntingtin cells.

How these changes in mitochondrial dynamics may contribute to increasing susceptibility of mutant huntingtin striatal cells to neurodegeneration? Oxidative stress as a consequence of dopamine metabolism results in the formation of reactive oxidative species and quinones that may affect several mitochondrial processes such as ATP production, membrane permeability or fission/fusion mitochondrial events [40–42]. Indeed, mitochondrial respiration and ATP production are significantly reduced in our HD striatal cell lines along with an increase in mitochondrial-generated reactive-oxidative species and a decrease in the mitochondrial membrane potential [43–46]. However, dopamine besides being an inductor of oxidative stress can also induce mitochondrial dysfunction through activation of dopamine receptors. Actually, activation of dopamine D2 receptors in mutant huntingtin striatal neurons alters mitochondrial function by down-regulating mitochondrial complex II expression [18] while mitochondrial axonal transport can be regulated by integration of the opposite effects of D1R and D2R activation [47]. Notably, there is no data on the potential role of dopamine receptors in mitochondrial fission-fusion events. In the present manuscript, we describe for the first time that D1R activation induces mitochondrial dynamics defects, leading to a percentage of striatal cells displaying mitochondrial fragmentation close to 80% when mHtt is expressed and to 40% in wild type conditions. The molecular mechanism underlying D1R-induced mitochondrial fragmentation either in wild-type or mutant huntingtin striatal cells involves an increase in Drp1 protein levels. However, two major differences can be noticed when mutant and wild-type cells are compared. First, in wild-type cells the increase in Drp1 levels was located in the cytosolic fraction while that in mutant huntingtin cells was found in the mitochondria and second, in mutant but not wild-type huntingtin cells the increase in Drp1 protein levels was accompanied by an increase in their GTPase activity, which agrees with the data on mitochondrial Drp1 localization. Altogether, these data suggest that D1R activation increases mHtt-induced mitochondrial fragmentation by altering Drp1 activity, which may be related with the higher susceptibility of mutant huntingtin striatal cells to D1R activation.

How D1R activation induces such changes in Drp1 levels, distribution and activity is a crucial question. Previous studies from our group have demonstrated that the increase in cell death induced by D1R activation in mutant huntingtin striatal cells is related with an increase in the activity of the Ser/Thr kinase Cdk5 [2]. Interestingly, Cdk5 has been involved in mitochondrial dysfunction by increasing oxidative stress [28] or acting as an upstream regulator of mitochondrial fragmentation [21]. In this scenario, we tried to integrate both pathways hypothesizing that in mutant huntingtin striatal cells the increase in Cdk5 activity induced by D1R activation was responsible for the increase in mitochondrial fragmentation. Supporting this hypothesis our data demonstrates that (1) inhibition of Cdk5 reduces Drp1 activity in mutant cells to levels similar to those found in wild-type cells, which was associated with a significant decrease in mitochondrial fragmentation and (2) prevents in mutant huntingtin cells the D1R-mediated increase of Drp1 protein levels and their translocation to the mitochondria. Translocation of Drp1 to the mitochondria is a critical event in mitochondrial fragmentation [48]. Even though the precise mechanisms underlying the recruitment of Drp1 to the mitochondria surface are not well understood several studies stress the role of Drp1 post-translational modifications [49]. Regarding regulation of Drp1 activity by phosphorylation the published data can be rather confusing, since phosphorylation at the same residue may result in induction or prevention of mitochondrial fission depending on cell type, physiological/pathological condition or even the kinase involved [50]. This is the case for Ser616. While in post-mitotic mature neurons and in physiological conditions phosphorylation at Ser616 by Cdk5 inhibits Drp1 activity and therefore mitochondrial fission [51], under pathological conditions, Ser616 (or Ser579 in Drp1 isoform

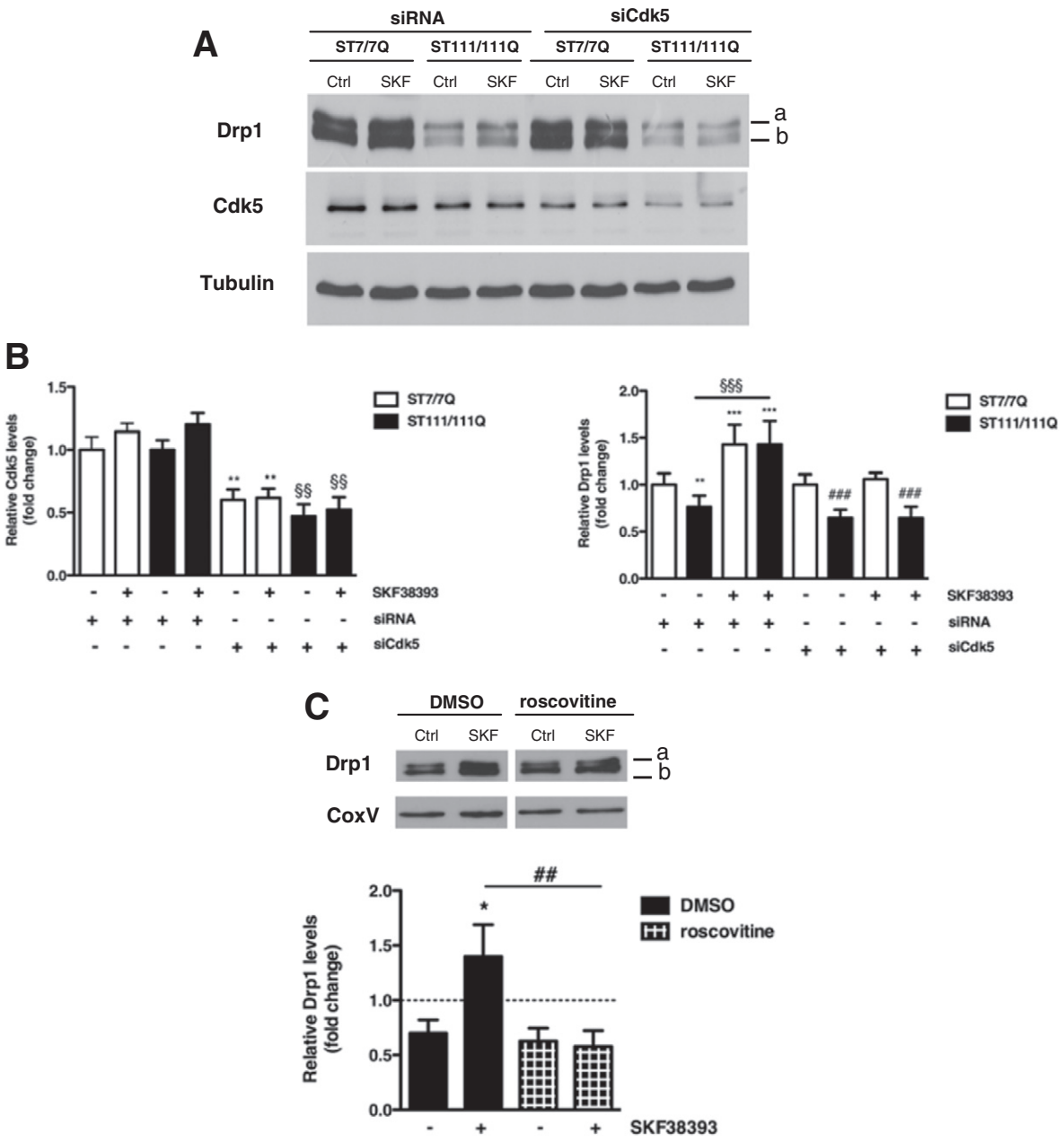

Fig. 9. Cdk5 promotes mitochondrial fission by altering the levels and the distribution of Drp1 in SKF 38393 treated ST111/111Q mutant cells. (A) Representative Western blots showing the levels of the fission protein Drp1 and Cdk5 in total extracts obtained from siRNA or siCdk5 transfected wild-type ST7/7Q and mutant ST111/111Q cells. α-Tubulin was used as loading control. When indicated, cells were treated with SKF 38393 (60 μM) during 1 h. Letters confer to the different isoforms recognized by the respective antibody (DRP1: a–b). (B) Bar histograms showing the relative fold change of Cdk5 and Drp1 protein levels in wild-type ST7/7Q and mutant ST111/111Q cells. Data represent mean ± SEM of 6 independent experiments. $^{***}p < 0.001$, $^{**}p < 0.01$ vs. vehicle-treated siRNA transfected ST7/7Q cells, $^{###}p < 0.001$ vs. vehicle-treated siCdk5 transfected ST7/7Q cells, $^{§§§}p < 0.001$ and $^{§§}p < 0.01$ vs. vehicle-treated siRNA transfected ST111/111Q cells as determined by One-way ANOVA with Newman–Keuls post hoc analysis. (C) Representative Western blots showing the levels of the fission protein Drp1 in mitochondrial fractions obtained from vehicle or roscovitine treated mutant ST111/111Q cells. When indicated, cells were treated with SKF 38393 (60 μM) during 1 h. CoxV was used as loading control. Letters indicate the different isoforms recognized by the respective antibody (DRP1: a–b). Bar histogram indicates the relative fold change ± SEM of 6 independent experiments; $^{*}p < 0.05$ vs. vehicle-treated ST111/111Q cells and $^{##}p < 0.01$ vs. roscovitine-treated ST111/111Q cells as determined by One-way ANOVA with Newman–Keuls post hoc analysis.

3) promotes mitochondrial fission either in mitotic or neuronal cells [52–54]. In our study, however, we have not observed any increase in phosphorylation at Ser616 in HD striatal cells compared to wild type cells (Supplementary Fig. 7) although Drp1 activity has been found to be increased suggesting that phosphorylation in other residues or other post-translational modifications could be involved. In this view, several studies have pointed out the role of the actin and microtubule cytoskeleton in Drp1-induced mitochondrial fission [48,55,56]. Interestingly, Cdk5 can phosphorylate a plethora of different proteins involved in cytoskeleton dynamics [57,58]. Indeed, increased Tau phosphorylation has been previously reported in mutant huntingtin striatal cells by our group [2] suggesting that an aberrant phosphorylation of cytoskeleton-related proteins could be involved in the accumulation of Drp1 in the mitochondria of mutant huntingtin striatal cells leading to mitochondrial fission.

5. Conclusion

In conclusion, we propose a model in which increased Cdk5 activity induced by both mHtt expression and aberrant dopaminergic signaling would contribute to increasing striatal susceptibility in HD by altering the expression, distribution and activity of Drp1 leading to mitochondrial fission events. Thus, our study contributes to the understanding of

the molecular mechanisms underlying striatal neurotoxicity in HD suggesting an important link between Cdk5 and Drp1 as mediators of dopaminergic-induced mitochondrial fragmentation in neurodegenerative diseases.

Supplementary data to this article can be found online at http://dx.doi.org/10.1016/j.bbadis.2015.06.025.

Transparency Document

The Transparency Document associated with this article can be found, in the online version.

Acknowledgments

We are very grateful to Ana Lopez and Maria Teresa Muñoz for technical assistance, Dr Teresa Rodrigo and the staff of the animal care facility (Facultat de Psicologia Universitat de Barcelona), Dr. Garikoitz Azkona and the staff of the animal care facility (Facultat de Medicina, Universitat de Barcelona) and Dr. Maria Calvo, Anna Bosch and Elisenda Coll from the Advanced Optical Microscopy Unit from Scientific and Technological Centers from University of Barcelona for their support and advice with confocal technique. We thank members of our laboratory for helpful discussion. This work was supported by grants from Ministerio de Economia y Competitividad (SAF2012-39142 to SG, SAF2014-57160-R to JA) projects integrated in *the Plan Nacional de I+D+I y cofinanciado por el Fondo Europeo de Desarrollo Regional* (*FEDER*); Cure Huntington's Disease Initiative (CHDI A-6146), Centro de Investigación Biomédicas en Red sobre Enfermedades Neurodegenerativas (CIBERNED CB06/05/0054 and CB06/05/0042), Fondo de Investigaciones Sanitarias Instituto de Salud Carlos III, *integrado en el Plan Nacional de I+D+I y cofinanciado por el ISCIII-Subdirección General de Evaluación y el Fondo Europeo de Desarrollo Regional* (*FEDER*) RD12/0019/0002 and Fundación Ramon Areces (CIVP16A1842).

References

[1] F. Trettel, D. Rigamonti, P. Hilditch-Maguire, V.C. Wheeler, A.H. Sharp, F. Persichetti, E. Cattaneo, M.E. MacDonald, Dominant phenotypes produced by the HD mutation in STHdh(Q111) striatal cells, Hum. Mol. Genet. 9 (2000) 2799–2809.
[2] P. Paoletti, I. Vila, M. Rife, J.M. Lizcano, J. Alberch, S. Gines, Dopaminergic and glutamatergic signaling crosstalk in Huntington's disease neurodegeneration: the role of p25/cyclin-dependent kinase 5, J. Neurosci. 28 (2008) 10090–10101.
[3] J. Yang, X. Liu, K. Bhalla, C.N. Kim, A.M. Ibrado, J. Cai, T.I. Peng, D.P. Jones, X. Wang, Prevention of apoptosis by Bcl-2: release of cytochrome c from mitochondria blocked, Science 275 (1997) 1129–1132.
[4] A. Giralt, M. Puigdellivol, O. Carreton, P. Paoletti, J. Valero, A. Parra-Damas, C.A. Saura, J. Alberch, S. Gines, Long-term memory deficits in Huntington's disease are associated with reduced CBP histone acetylase activity, Hum. Mol. Genet. 21 (2012) 1203–1216.
[5] W.J. Koopman, H.J. Visch, J.A. Smeitink, P.H. Willems, Simultaneous quantitative measurement and automated analysis of mitochondrial morphology, mass, potential, and motility in living human skin fibroblasts, Cytometry A 69 (2006) 1–12.
[6] J.R. Hom, J.S. Gewandter, L. Michael, S.S. Sheu, Y. Yoon, Thapsigargin induces biphasic fragmentation of mitochondria through calcium-mediated mitochondrial fission and apoptosis, J. Cell. Physiol. 212 (2007) 498–508.
[7] T.H.s.D.C.R. Group, A novel gene containing a trinucleotide repeat that is expanded and unstable on Huntington's disease chromosomes, Cell 72 (1993) 971–983.
[8] C.A. Ross, R.L. Margolis, Huntington's disease, Clin. Neurosci. Res. 1 (2001) 142–152.
[9] J.B. Martin, J.F. Gusella, Huntington's disease. Pathogenesis and management, N. Engl. J. Med. 315 (1986) 1267–1276.
[10] A.V. Panov, C.A. Gutekunst, B.R. Leavitt, M.R. Hayden, J.R. Burke, W.J. Strittmatter, J.T. Greenamyre, Early mitochondrial calcium defects in Huntington's disease are a direct effect of polyglutamines, Nat. Neurosci. 5 (2002) 731–736.
[11] A.L. Orr, S. Li, C.E. Wang, H. Li, J. Wang, J. Rong, X. Xu, P.G. Mastroberardino, J.T. Greenamyre, X.J. Li, N-terminal mutant huntingtin associates with mitochondria and impairs mitochondrial trafficking, J. Neurosci. 28 (2008) 2783–2792.
[12] M.F. Beal, Aging, energy, and oxidative stress in neurodegenerative diseases, Ann. Neurol. 38 (1995) 357–366.
[13] F. Mochel, R.G. Haller, Energy deficit in Huntington disease: why it matters, J. Clin. Invest. 121 (2011) 493–499.
[14] T. Milakovic, R.A. Quintanilla, G.V. Johnson, Mutant huntingtin expression induces mitochondrial calcium handling defects in clonal striatal cells: functional consequences, J. Biol. Chem. 281 (2006) 34785–34795.
[15] D. Lim, L. Fedrizzi, M. Tartari, C. Zuccato, E. Cattaneo, M. Brini, E. Carafoli, Calcium homeostasis and mitochondrial dysfunction in striatal neurons of Huntington disease, J. Biol. Chem. 283 (2008) 5780–5789.
[16] H. Wang, P.J. Lim, M. Karbowski, M.J. Monteiro, Effects of overexpression of huntingtin proteins on mitochondrial integrity, Hum. Mol. Genet. 18 (2009) 737–752.
[17] U. Shirendeb, A.P. Reddy, M. Manczak, M.J. Calkins, P. Mao, D.A. Tagle, P.H. Reddy, Abnormal mitochondrial dynamics, mitochondrial loss and mutant huntingtin oligomers in Huntington"s disease: implications for selective neuronal damage, Hum. Mol. Genet. 20 (2011) 1438–1455.
[18] A. Benchoua, Y. Trioulier, E. Diguet, C. Malgorn, M.C. Gaillard, N. Dufour, J.M. Elalouf, S. Krajewski, P. Hantraye, N. Deglon, E. Brouillet, Dopamine determines the vulnerability of striatal neurons to the N-terminal fragment of mutant huntingtin through the regulation of mitochondrial complex II, Hum. Mol. Genet. 17 (2008) 1446–1456.
[19] T.S. Tang, X. Chen, J. Liu, I. Bezprozvanny, Dopaminergic signaling and striatal neurodegeneration in Huntington's disease, J. Neurosci. 27 (2007) 7899–7910.
[20] J.H. Weishaupt, L. Kussmaul, P. Grotsch, A. Heckel, G. Rohde, H. Romig, M. Bahr, F. Gillardon, Inhibition of CDK5 is protective in necrotic and apoptotic paradigms of neuronal cell death and prevents mitochondrial dysfunction, Mol. Cell. Neurosci. 24 (2003) 489–502.
[21] K. Meuer, I.E. Suppanz, P. Lingor, V. Planchamp, B. Goricke, L. Fichtner, G.H. Braus, G.P. Dietz, S. Jakobs, M. Bahr, J.H. Weishaupt, Cyclin-dependent kinase 5 is an upstream regulator of mitochondrial fission during neuronal apoptosis, Cell Death Differ. 14 (2007) 651–661.
[22] E. Bossy-Wetzel, M.J. Barsoum, A. Godzik, R. Schwarzenbacher, S.A. Lipton, Mitochondrial fission in apoptosis, neurodegeneration and aging, Curr. Opin. Cell Biol. 15 (2003) 706–716.
[23] J.M. Oliveira, M.B. Jekabsons, S. Chen, A. Lin, A.C. Rego, J. Goncalves, L.M. Ellerby, D.G. Nicholls, Mitochondrial dysfunction in Huntington's disease: the bioenergetics of isolated and in situ mitochondria from transgenic mice, J. Neurochem. 101 (2007) 241–249.
[24] V. Costa, M. Giacomello, R. Hudec, R. Lopreiato, G. Ermak, D. Lim, W. Malorni, K.J. Davies, E. Carafoli, L. Scorrano, Mitochondrial fission and cristae disruption increase the response of cell models of Huntington's disease to apoptotic stimuli, EMBO Mol. Med. 2 (2010) 490–503.
[25] J. Bereiter-Hahn, M. Voth, Dynamics of mitochondria in living cells: shape changes, dislocations, fusion, and fission of mitochondria, Microsc. Res. Tech. 27 (1994) 198–219.
[26] Y.N. Jin, Y.V. Yu, S. Gundemir, C. Jo, M. Cui, K. Tieu, G.V. Johnson, Impaired mitochondrial dynamics and Nrf2 signaling contribute to compromised responses to oxidative stress in striatal cells expressing full-length mutant huntingtin, PLoS One 8 (2013) e57932.
[27] W. Song, J. Chen, A. Petrilli, G. Liot, E. Klinglmayr, Y. Zhou, P. Poquiz, J. Tjong, M.A. Pouladi, M.R. Hayden, E. Masliah, M. Ellisman, I. Rouiller, R. Schwarzenbacher, B. Bossy, G. Perkins, E. Bossy-Wetzel, Mutant huntingtin binds the mitochondrial fission GTPase dynamin-related protein-1 and increases its enzymatic activity, Nat. Med. 17 (2011) 377–382.
[28] K.H. Sun, Y. de Pablo, F. Vincent, K. Shah, Deregulated Cdk5 promotes oxidative stress and mitochondrial dysfunction, J. Neurochem. 107 (2008) 265–278.
[29] T.G. Hastings, The role of dopamine oxidation in mitochondrial dysfunction: implications for Parkinson's disease, J. Bioenerg. Biomembr. 41 (2009) 469–472.
[30] S. Jana, M. Sinha, D. Chanda, T. Roy, K. Banerjee, S. Munshi, B.S. Patro, S. Chakrabarti, Mitochondrial dysfunction mediated by quinone oxidation products of dopamine: implications in dopamine cytotoxicity and pathogenesis of Parkinson's disease, Biochim. Biophys. Acta 1812 (2011) 663–673.
[31] A.M. Labrousse, M.D. Zappaterra, D.A. Rube, A.M. van der Bliek, *C. elegans* dynamin-related protein DRP-1 controls severing of the mitochondrial outer membrane, Mol. Cell 4 (1999) 815–826.
[32] E. Smirnova, L. Griparic, D.L. Shurland, A.M. van der Bliek, Dynamin-related protein Drp1 is required for mitochondrial division in mammalian cells, Mol. Biol. Cell 12 (2001) 2245–2256.
[33] Z.H. Sheng, Q. Cai, Mitochondrial transport in neurons: impact on synaptic homeostasis and neurodegeneration, Nat. Rev. Neurosci. 13 (2012) 77–93.
[34] R.A. Quintanilla, G.V.W. Johnson, Role of mitochondrial dysfunction in the pathogenesis of Huntington's disease, Brain Res. Bull. 80 (2009) 242–247.
[35] V. Costa, L. Scorrano, Shaping the role of mitochondria in the pathogenesis of Huntington's disease, EMBO J. 31 (2012) 1853–1864.
[36] P.H. Reddy, Increased mitochondrial fission and neuronal dysfunction in Huntington's disease: implications for molecular inhibitors of excessive mitochondrial fission, Drug Discov. Today 19 (2014) 951–955.
[37] J. Li, S. Donath, Y. Li, D. Qin, B.S. Prabhakar, P. Li, miR-30 regulates mitochondrial fission through targeting p53 and the dynamin-related protein-1 pathway, PLoS Genet. 6 (2010) e1000795.
[38] J.S. Steffan, A. Kazantsev, O. Spasic-Boskovic, M. Greenwald, Y.Z. Zhu, H. Gohler, E.E. Wanker, G.P. Bates, D.E. Housman, L.M. Thompson, The Huntington's disease protein interacts with p53 and CREB-binding protein and represses transcription, Proc. Natl. Acad. Sci. U. S. A. 97 (2000) 6763–6768.
[39] U.P. Shirendeb, M.J. Calkins, M. Manczak, V. Anekonda, B. Dufour, J.L. McBride, P. Mao, P.H. Reddy, Mutant huntingtin's interaction with mitochondrial protein Drp1 impairs mitochondrial biogenesis and causes defective axonal transport and synaptic degeneration in Huntington's disease, Hum. Mol. Genet. 21 (2012) 406–420.
[40] S. Wu, F. Zhou, Z. Zhang, D. Xing, Mitochondrial oxidative stress causes mitochondrial fragmentation via differential modulation of mitochondrial fission–fusion proteins, FEBS J. 278 (2011) 941–954.
[41] S.B. Berman, T.G. Hastings, Dopamine oxidation alters mitochondrial respiration and induces permeability transition in brain mitochondria: implications for Parkinson's disease, J. Neurochem. 73 (1999) 1127–1137.

[42] M. Frank, S. Duvezin-Caubet, S. Koob, A. Occhipinti, R. Jagasia, A. Petcherski, M.O. Ruonala, M. Priault, B. Salin, A.S. Reichert, Mitophagy is triggered by mild oxidative stress in a mitochondrial fission dependent manner, Biochim. Biophys. Acta 1823 (2012) 2297–2310.
[43] T. Milakovic, G.V. Johnson, Mitochondrial respiration and ATP production are significantly impaired in striatal cells expressing mutant huntingtin, J. Biol. Chem. 280 (2005) 30773–30782.
[44] M. Ribeiro, T.R. Rosenstock, T. Cunha-Oliveira, I.L. Ferreira, C.R. Oliveira, A.C. Rego, Glutathione redox cycle dysregulation in Huntington's disease knock-in striatal cells, Free Radic. Biol. Med. 53 (2012) 1857–1867.
[45] I.S. Seong, E. Ivanova, J.M. Lee, Y.S. Choo, E. Fossale, M. Anderson, J.F. Gusella, J.M. Laramie, R.H. Myers, M. Lesort, M.E. MacDonald, HD CAG repeat implicates a dominant property of huntingtin in mitochondrial energy metabolism, Hum. Mol. Genet. 14 (2005) 2871–2880.
[46] R.A. Quintanilla, Y.N. Jin, K. Fuenzalida, M. Bronfman, G.V. Johnson, Rosiglitazone treatment prevents mitochondrial dysfunction in mutant huntingtin-expressing cells: possible role of peroxisome proliferator-activated receptor-gamma (PPARgamma) in the pathogenesis of Huntington disease, J. Biol. Chem. 283 (2008) 25628–25637.
[47] S. Chen, G.C. Owens, D.B. Edelman, Dopamine inhibits mitochondrial motility in hippocampal neurons, PLoS ONE 3 (2008) e2804.
[48] L.A. Pon, Mitochondrial fission: rings around the organelle, Curr. Biol. 23 (2013) R279–R281.
[49] C.R. Chang, C. Blackstone, Dynamic regulation of mitochondrial fission through modification of the dynamin-related protein Drp1, Ann. N. Y. Acad. Sci. 1201 (2010) 34–39.
[50] B. Cho, S.Y. Choi, H.M. Cho, H.J. Kim, W. Sun, Physiological and pathological significance of dynamin-related protein 1 (drp1)-dependent mitochondrial fission in the nervous system, Exp. Neurobiol. 22 (2013) 149–157.
[51] B. Cho, H.M. Cho, H.J. Kim, J. Jeong, S.K. Park, E.M. Hwang, J.Y. Park, W.R. Kim, H. Kim, W. Sun, CDK5-dependent inhibitory phosphorylation of Drp1 during neuronal maturation, Exp. Mol. Med. 46 (2014) e105.
[52] N. Taguchi, N. Ishihara, A. Jofuku, T. Oka, K. Mihara, Mitotic phosphorylation of dynamin-related GTPase Drp1 participates in mitochondrial fission, J. Biol. Chem. 282 (2007) 11521–11529.
[53] X. Qi, M.H. Disatnik, N. Shen, R.A. Sobel, D. Mochly-Rosen, Aberrant mitochondrial fission in neurons induced by protein kinase C{delta} under oxidative stress conditions in vivo, Mol. Biol. Cell 22 (2011) 256–265.
[54] A. Jahani-Asl, E. Huang, I. Irrcher, J. Rashidian, N. Ishihara, D.C. Lagace, R.S. Slack, D.S. Park, CDK5 phosphorylates DRP1 and drives mitochondrial defects in NMDA-induced neuronal death, Hum. Mol. Genet. (2015 (pii: ddv188, Epub ahead of print)).
[55] K.J. De Vos, V.J. Allan, A.J. Grierson, M.P. Sheetz, Mitochondrial function and actin regulate dynamin-related protein 1-dependent mitochondrial fission, Curr. Biol. 15 (2005) 678–683.
[56] A. Varadi, Cytoplasmic dynein regulates the subcellular distribution of mitochondria by controlling the recruitment of the fission factor dynamin-related protein-1, J. Cell Sci. 117 (2004) 4389–4400.
[57] T. Kawauchi, Cdk5 regulates multiple cellular events in neural development, function and disease, Develop. Growth Differ. 56 (2014) 335–348.
[58] E. Contreras-Vallejos, E. Utreras, D.A. Borquez, M. Prochazkova, A. Terse, H. Jaffe, A. Toledo, C. Arruti, H.C. Pant, A.B. Kulkarni, C. Gonzalez-Billault, Searching for novel Cdk5 substrates in brain by comparative phosphoproteomics of wild type and Cdk5 −/− mice, PLoS One 9 (2014) e90363.